frequencies in three different models (genotype, dominant, and recessive forms) of each case group with controls. In the allelic model, the allelic frequencies were compared between cases and controls using a 2×2 contingency table. In the genotype model, the frequencies of the three genotypes were compared using a 2×3 contingency table, in the dominant model, the frequencies of the homozygote for the non-risk allele were compared using a 2×2 contingency table, and in the recessive model, the frequencies of the homozygote for the risk allele were compared using a 2×2 contingency table. Also, association analysis was performed with the use of the Cochran–Armitage trend test. After statistical analysis in three different models (genotype, recessive, and dominant model) and trend test, the minimum p value of each SNPs were obtained from lowest p value of these tests. The minimum p values were used to test whether they were lower than the significance levels. Odds ratios (ORs) with 95% confidence intervals (CIs) were estimated for the effects of risk allele and also for both the dominant and recessive forms of the genotypes. To account for multiple statistical testing, the false discovery rate (FDR) was calculated based on the minimum p values from each typical type of AMD and PCV case-control study by the method of Benjamini and Hochberg [53], and it was employed at a significance level of 0.05. Pair wise SNP linkage disequilibrium (LD) values were calculated from the genotype data using Haploview ver.4.0.

Logistic regression analysis and calculation of joint OR

Logistic regression analysis was performed to assess the joint contributions of the three candidate SNPs (rs800292, rs10490924, and rs2241394) to the risk of typical wet-type AMD or PCV using R software. To model the genetic effects, we adopted the following three genetic models with classification variables: the 2-genotype model (AA+AB and BB or AA and AB+BB) and the 3-genotype model (AA, AB, and BB). The logistic regression models were compared by the Akaike information criterion (AIC) to obtain the best-fitting model with the lowest AIC. Univariate logistic regression analysis was initially carried out for three genotype models on each SNPs, and multivariate analysis was then performed. The logistic regression models for all the possible combinations of SNPs were compared by the AIC to obtain the best-fitting model with the lowest AIC. Joint ORs for pairs of loci (rs10490924 and rs800292; rs10490924 and rs2241394; rs10490924 and rs2241394) were calculated for each 2-locus genotype separately, using the non-risk double homozygote genotype as a reference. The estimation of joint ORs was carried out with the R package Epitools. This analysis added 0.5 to each cell in a case including 0 in contingency table [54].

Results

Genotyping of typical wet-type AMD and PCV

We conducted genotyping on DNA samples obtained from Japanese patients with typical wet-type AMD and PCV. To increase the power of detecting genetic difference, we selected samples from AMD cases at stage 5b, at least in one eye without PCV, for typical wet-type AMD analysis. Stage 5 is defined as exudative AMD, including nondrusenoid pigment epithelial detachments, serious or hemorrhage retinal detachments, choroidal neovascular membrane with subretinal or sub-RPE hemorrhages or fibrosis, or scars consistent with treatment of AMD. AMD with choroidal neovascular membrane or disciform scar is defined as stage 5b [51]. Although the controls were age-matched (Table 1), the gender of the population was biased because of the characteristically higher incidence of men in Japanese AMD population [6]. One hundred cases versus 190 controls were genotyped for 500,568 tag-SNPs using the Affymetrix Human Mapping 500 K Array Set. For typical AMD, statistical analysis was performed for a selected 314,950 tag-SNPs through quality control filters (HWE $p<0.0001$, minor allele frequency <5%, and call rate <90%) to reduce low-quality signal. These SNPs are shown in Fig. 1a and b, and the 77 SNPs associated with typical wet-type AMD with genotypic p values<0.0001 are listed in the Supplementary Table S1. Our study identified several genomic locations as being potentially associated with AMD risk. Among these SNPs, rs10490924, rs3750848, and rs2672587 with false discovery rate <0.05 (Benjamini–Hochberg method) were significantly associated with typical wet-type AMD in Japanese patients with a minimum p value of 4.1×10^{-14}, 4.6×10^{-14} and 2.2×10^{-9}, respectively (Table 2). For PCV, statistical analysis was performed for 313,772 quality controlled filtered SNPs. These SNPs are shown in Fig. 1c, d, and the 98 SNPs associated with PCV with genotypic p values< 0.0001 are listed in Supplementary Table S2. Two SNPs: rs10490924 and rs3750848 are statistically associated with PCV with a minimum p value of 3.7×10^{-8} and 2.4×10^{-8}, respectively. These results confirm a strong association of the *AMRS2/HTRA1* gene region with both typical wet-type AMD and PCV in Japanese, however, we could not comprehensively evaluate the association between Japanese AMD and complement related genes probably due to the low statistical power by this method.

Analysis of the SNPs in *ARMS2/HTRA1*, *CFH*, *C2/BF*, *C3*, and *CFI* gene regions

Despite the success of many genome wide association study published, not all the genome wide screening data are analyzed to their full potential. Thus, recently the advantage

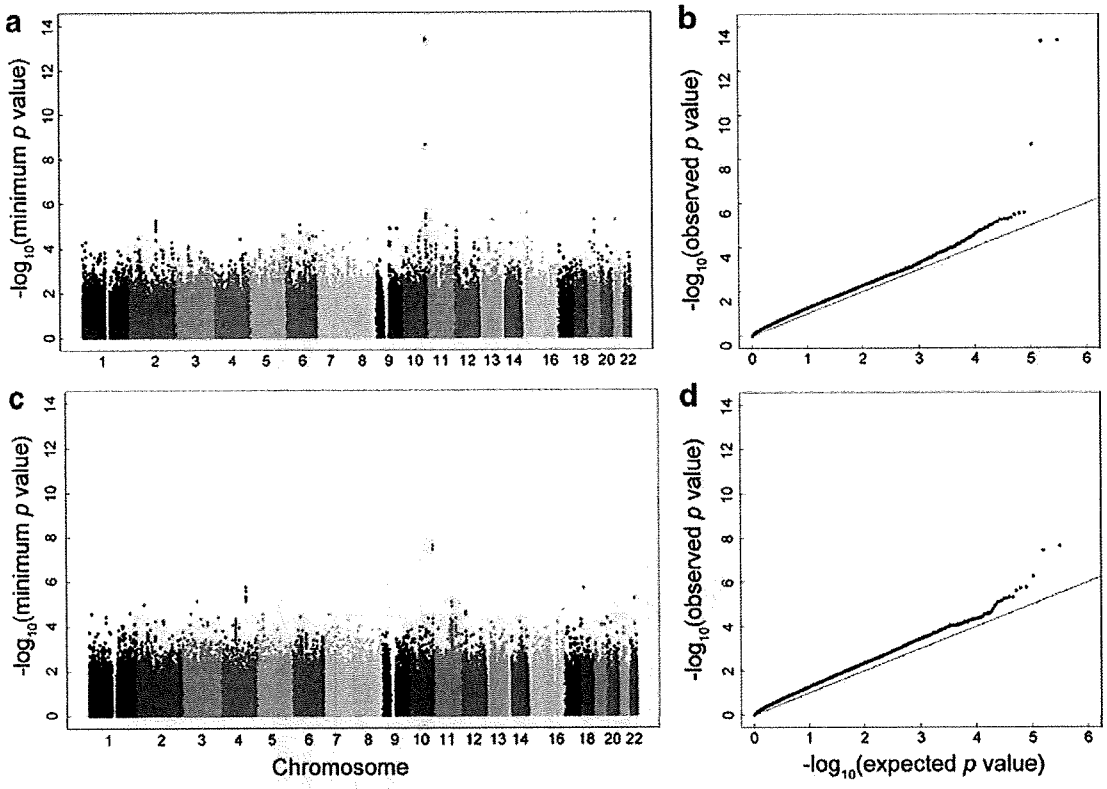

Fig. 1 Genome wide screening for Japanese typical wet-type AMD and PCV. Whole-genome association analyasis of typical wet-type AMD (**a**) and PCV (**c**). The scatter plots were drawn for $-\log_{10}$ (minimum p value) against SNP position in the chromosomes. Quantile-quantile plot for association results of typical wet-type AMD (**b**) and PCV (**d**). The distribution of observed p values versus expected p values. *Dots* represent all the 314950 SNPs and 313772 SNPs analyzed for association studies for typical wet-type AMD and PCV, respectively

of association analysis on candidate genes selected by certain criteria has been proposed. We extracted genotyping data in gene regions, which were associated with typical wet-type AMD in Caucasian populations, namely *ARMS2/HTRA1*, *CFH*, *C2/BF*, *C3*, and *CFI*. Using *Taq*Man analysis, we additionally genotyped four SNPs; rs800292 (*CFH*), rs547154 (*C2*), rs2230199 (*C3*), and rs10033900 (*CFI*), which were significantly associated with Caucasian typical wet-type AMD but were not covered in the Affymetrix Human Mapping 500 K Array. rs800292 shows association with both typical wet-type AMD and PCV ($10^{-4}<p<10^{-3}$, Table 2) as reported previously [39, 44]. No difference in genetic frequency between case and control was detected for rs547154, rs10033900, and rs2230199. After Benjamini–Hochberg correction, 12 and seven SNPs showing significant association with typical wet-type AMD and PCV, respectively (Table 2, Fig. 2), were found at the threshold FDR <0.05. For typical wet-type AMD, four SNPs in the *CFH* gene region including rs800292 appeared to be significantly associated following the *ARMS2/HTRA1* gene region. While in PCV, rs800292 in the *CFH* gene region and rs2241394 in the *C3* gene region were significantly associated with the *ARMS2/HTRA1* gene region. These results indicate common and distinctive aspects of genetic background between typical wet-type AMD and PCV in Japanese population. We also used logistic regression to further compare the genetic risk properties of typical wet-type AMD and PCV. Table 3 summarizes the best-fit and most parsimonious model analyzed by logistic regression, which was used to explore the joint contributions of the three candidate SNPs (rs800292, rs10490924, and rs2241394) to the risk of typical wet-type AMD and PCV. The AIC for three genetic models of the candidate SNPs were compared, followed by logistic regression analysis to assess the joint contributions of the genetic models with the lowest AIC. These results suggest that the joint effect of rs800292, rs10490924, and rs2241394 best described the risk for development of PCV. However, an effect of rs2241394 was not observed for typical wet-type AMD. Independent and joint ORs of typical wet-type AMD combining the genotypes from the rs800292 and rs10490924 or PCV for the two variants among rs800292, rs10490924 and rs2241394 were estimated (Table 4). When three SNPs were combined, some values

Table 2 Statistically significant SNPs associated with typical wet-type AMD and PCV from analysis of candidate gene

dbSNP ID (A/B)	Chr.	Position	Associated gene	SNP type	Case			Control			*p* value			Odds ratio (95% CI)		
					AA	AB	BB	AA	AB	BB	Allele	Minimum	Model	Allele	Recessive	Dominant
AMD																
rs800292 (G/A)	1	194,908,856	*CFH*	Exon	47	46	3	60	92	36	1.2×10^{-4}	7.4×10^{-5}	Genotype	2.08 (1.43 –3.04)	7.34 (2.20 –24.52)	2.05 (1.24–3.39)
rs1329423 (G/A)	1	194,913,010	*CFH*	Intron	35	50	15	47	87	55	0.0066	0.0049	Trend	1.63 (1.15 –2.31)	2.33 (1.24 –4.38)	1.63 (0.96–2.76)
rs10737680 (T/G)	1	194,946,078	*CFH*	Intron	43	49	8	58	88	44	0.0014	0.0012	Dominant	1.79 (1.25 –2.56)	3.47 (1.56 –7.69)	1.72 (1.04–2.84)
rs742855 (G/A	1	194,972,143	*CFH*	Intron	30	54	16	46	84	59	0.0183	0.0059	Dominant	1.52 (1.08 –2.15)	2.38 (1.29 –4.42)	1.33 (0.78–2.29)
rs2736911 (G/A)	10	124,204,345	*HTRA1*	−6,686	80	20	0	108	74	6	1.1×10^{-4}	4.8×110^{-5}	Trend	2.67 (1.59 –4.49)	NA	2.96 (1.68 –5.23)
rs10490924 (A/C)	10	124,204,438	*HTRA1*	−6,593	52	30	18	20	84	85	4.5×10^{-15}	4.1×10^{-14}	Recessive	4.16 (2.89 –5.99)	3.72 (2.07 –6.68)	9.15 (4.99 –16.80)
rs3750848 (C/A)	10	124,205,305	*HTRA1*	−5,726	52	30	18	20	84	84	5.1×10^{-15}	4.6×10^{-14}	Recessive	4.13 (2.86 –5.94)	3.68 (2.05 –6.61)	9.10 (4.96 –16.70)
rs11200644 (A/G)	10	124,220,931	*HTRA1*	Intron	76	23	0	105	79	6	3.9×10^{-4}	1.7×10^{-4}	Trend	2.40 (1.46 –3.93)	NA	2.67 (1.55 –4.62)
rs7093894 (C/A)	10	124,224,870	*HTRA1*	Intron	73	27	0	88	86	15	4.2×10^{-6}	3.0×10^{-6}	Trend	2.84 (1.79 –4.50)	NA	3.10 (1.83 –5.25)
rs2672587 (C/G)	10	124,225,345	*HTRA1*	Intron	47	38	15	29	85	74	2.0×10^{-10}	2.2×10^{-9}	Trend	3.16 (2.21 –4.53)	3.68 (1.97 –6.85)	4.86 (2.78 –8.49)
rs2250804 (G/A)	10	124,254,868	*HTRA1*	Intron	27	48	25	16	97	76	1.2×10^{-4}	7.1×10^{-5}	Recessive	2.01 (1.42 –2.85)	2.02 (1.18 –3.46)	4.00 (2.03 –7.86)
rs2268356 (G/A)	10	124,255,316	*HTRA1*	Intron	47	40	12	59	104	24	0.057	0.0068	Recessive	1.43 (1.00 –2.06)	1.07 (0.51 –2.24)	1.96 (1.19 –3.24)
PCV																
rs800292 (G/A)	1	194,908,856	*CFH*	Exon	5	43	47	36	92	60	3.4×10^{-4}	2.6×10^{-4}	Trend	2.00 (1.37 –2.92)	4.26 (1.61 –11.26)	2.09 (1.26 –3.46)
rs10490924 (A/C)	10	124,204,438	*HTRA1*	−6,593	32	50	18	20	84	85	3.0×10^{-8}	3.7×10^{-8}	Trend	2.72 (1.91 –3.86)	3.72 (2.07 –6.68)	3.98 (2.13 –7.43)
rs3750848 (C/A)	10	124,205,305	*HTRA1*	−5,726	17	50	32	84	84	20	1.7×10^{-8}	2.4×10^{-8}	Trend	2.76 (1.93 –3.93)	3.90 (2.15 –7.07)	4.01 (2.14 –7.51)
rs11200644 (A/G)	10	124,220,931	*HTRA1*	Intron	72	26	2	105	79	6	0.0132	0.0055	Recessive	1.78 (1.13 –2.81)	1.60 (0.32 –8.07)	2.08 (1.24 –3.51)
rs7093894 (C/A)	10	124,224,870	*HTRA1*	Intron	4	29	67	15	86	88	0.0015	0.0012	Recessive	1.95 (1.28)	2.07 (0.67 –6.41)	2.33 (1.41 –3.86)
rs2672587 (C/G)	10	124,225,345	*HTRA1*	Intron	26	55	18	29	85	74	2.8×10^{-4}	2.5×10^{-4}	Trend	1.92 (1.35 –2.71)	2.92 (1.62 –5.26)	1.95 (1.07 –9.55)
rs2241394 (G/C)	19	6,636,260	*C3*	Intron	0	6	93	2	33	154	0.0025	0.0037	Trend	3.47 (1.48 –8.38)	NA	3.52 (1.43 –8.69)

Allele *p* values were obtained from Fisher's exact test. Minimum *p* values were obtained from lowest *p* value of Fisher's exact test for three disease-risk models (genotype, dominant, and recessive model) and Cochran-Armitage trend test. Model showed the genetic model which minimum *p* value was found in. *AMD* typical wet-type AMD, *Chr.* chromosome number, *A* risk allele, *B* non-risk allele, *CI* confidence interval

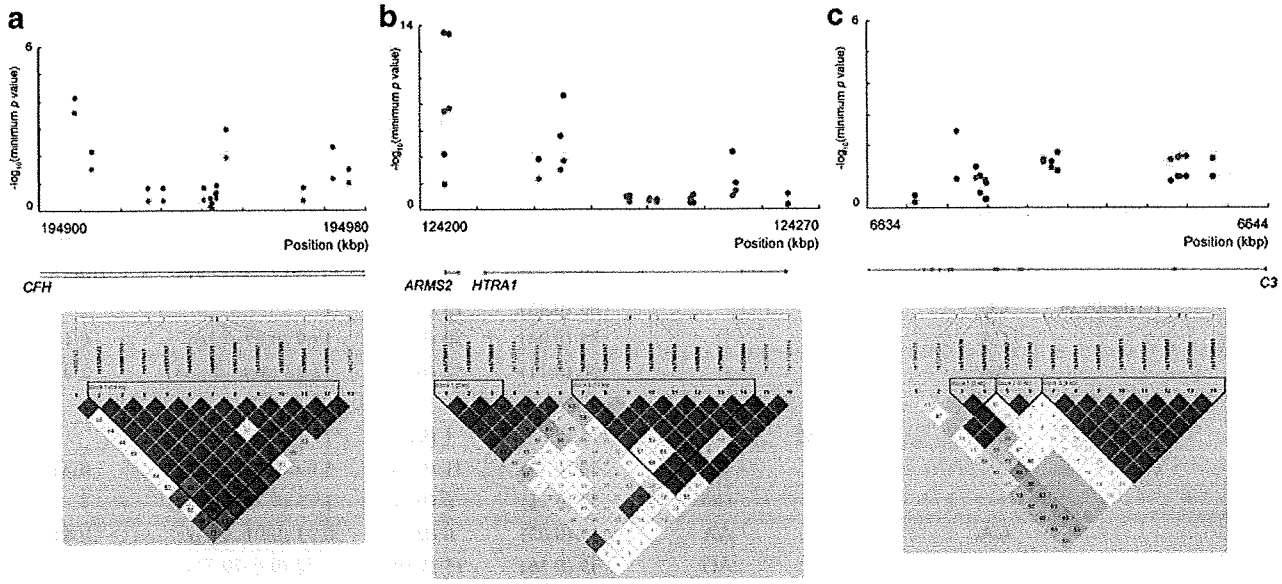

Fig. 2 Schematic view of association and LD results from association analysis for typical wet-type AMD and PCV in the significantly associated region. *Upper panel*, SNPs association results in the chromosome 1 (**a**), chromosome 10 (**b**), and chromosome 19 (**c**). This panel shows *p* values for association testing drawn from the candidate genes focused study including results using *Taq*man genotyping assay. Known genes in the area are shown. *Down panel*, LD structure of each region. Pairwise LD was calculated from all the data set in this study using the methods of Gabriel as implemented in Haploview. In each *box* are shown are the LD relationships between each SNP pair using Haploview's standard color scheme. *Blue circles*, typical wet-type AMD; *Red circles*, PCV

appeared to be unreliable because of small numbers of individuals in some of the genotype combinations. Therefore, two SNPs were analyzed. The heterozygous (CA) risk genotype of rs10490924 was detected more often in PCV cases than in controls with *p* value of 0.0008 and OR of 2.8 (95% CI=1.5–5.2), however the difference in the frequency of the heterozygous (CA) at the same loci between typical wet-type AMD cases and controls did not reach statistical significance. Both typical wet-type AMD and PCV cases carried the rs800292 heterozygous (AG) and homozygous

Table 3 Calculation of AIC by logistic regression analysis in three genotype models

dbSNP ID	Model	AMD		PCV	
		AIC	AIC difference	AIC	AIC difference
Single					
rs800292	Gen	349.6		352.1	
	Rec	350.4		353.8	
	Dom	359.6		357	
rs10490924	Gen	317.9		347.8	
	Rec	354.7		354.7	
	Dom	318.4		357.4	
rs2241394	Gen	375.4		366.7	
	Rec	345.1		373	
	Dom	374.7		365.3	
Joint					
rs800292gen + rs10490924gen		291.8	0	325.9	5.5
rs800292gen + rs2241394dom		349.2	57.4	344	23.6
rs10490924gen + rs2241394dom		319.2	27.4	344	23.6
rs800292gen + rs10490924gen + rs2241394dom		293.4	1.6	320.4	0

AMD typical wet-type AMD, *Gen* genotype model, *Rec* recessive model, *Dom* dominant model, *AIC* Akaike information criterion (the AIC difference is the difference from the AIC of the best fitting model)

Table 4 Two-locus odds ratios and *p* values for different genotypic combinations of the rs800292, rs10490924, and rs2241394 polymorphisms

Genotype combination					Number (%)			
					Control	Case	Odds ratio (95%CI)	*p* value
AMD	Single							
	rs800292	AA			36 (0.19)	3 (0.03)	1	
		AG			92 (0.49)	46 (0.48)	6.00 (1.75–20.52)	0.0011
		GG			60 (0.32)	47 (0.49)	9.40 (2.73–32.42)	2.3×10^{-5}
	rs10490924	CC			85 (0.45)	18 (0.18)	1	
		CA			84 (0.44)	30 (0.3)	1.69 (0.87–3.26)	0.1411
		AA			20 (0.11)	52 (0.52)	12.28 (5.95–25.33)	2.9×10^{-13}
	Joint							
	rs10490924	CC	rs800292	AA	15 (0.05)	1 (0)	1	
				AG	38 (0.13)	11 (0.04)	3.09 (0.51–18.69)	0.3234
				GG	32 (0.11)	5 (0.02)	1.75 (0.26–11.74)	1
		CA		AA	15 (0.05)	0 (0)	0.33 (0.01–8.83)	0.4866
				AG	45 (0.16)	15 (0.05)	3.52 (0.6–20.71)	0.3353
				GG	23 (0.08)	14 (0.05)	6.38 (1.05–38.54)	0.061
		AA		AA	6 (0.02)	2 (0.01)	3.97 (0.43–36.66)	0.5633
				AG	8 (0.03)	20 (0.07)	24.92 (3.89–159.6)	7.1×10^{-5}
				GG	5 (0.02)	28 (0.1)	53.55 (7.94–361.02)	
PCV	Single							
	rs800292	GG			36 (0.19)	5 (0.05)	1	
		GA			92 (0.49)	43 (0.45)	3.37 (1.23–9.18)	0.0156
		AA			60 (0.32)	47 (0.49)	5.64 (2.05–15.49)	
	rs10490924	CC			85 (0.45)	18 (0.18)	1	
		CA			84 (0.44)	50 (0.5)	2.81 (1.52–5.21)	0.0008
		AA			20 (0.11)	32 (0.32)	7.56 (3.55–16.08)	6.0×10^{-8}
	rs2241394	CC + CG			35 (0.19)	6 (0.06)	1	
		GG			154 (0.81)	93 (0.94)	3.52 (1.43–8.69)	0.0041
	Joint							
	rs10490924	CC	rs80092	AA	15 (0.05)	0 (0)	1	
				AG	38 (0.13)	7 (0.02)	6.04 (0.32–112.28)	0.0994
				GG	32 (0.11)	11 (0.04)	10.97 (0.61–198.43)	0.0253
		CA		AA	15 (0.05)	4 (0.01)	9.00 (0.45–181.74)	0.1131
				AG	45 (0.16)	24 (0.09)	16.69 (0.96–291.08)	0.0043
				GG	23 (0.08)	21 (0.07)	28.36 (1.6–503.36)	0.0005
		AA		AA	6 (0.02)	1 (0)	7.15 (0.26–199.68)	0.1014
				AG	8 (0.03)	12 (0.04)	45.59 (2.39–869.16)	0.0002
				GG	5 (0.05)	15 (0.05)	87.36 (4.44–1,719.03)	4.6×10^{-6}
	rs10490924	CC	rs2241394	CC+CG	15 (0.08)	2 (0.02)	1	
				GG	70 (0.37)	16 (0.16)	1.71 (0.36–8.26)	0.7302
		CA		CC+CG	17 (0.09)	2 (0.02)	0.88 (0.11–7.06)	1
				GG	67 (0.35)	48 (0.48)	5.37 (1.17–24.6)	0.0172
		AA		CC+CG	3 (0.02)	2 (0.02)	5.00 (0.49–50.83)	0.2098
				GG	17 (0.09)	29. (0.29)	12.79 (2.6–62.88)	0.0004

AMD, typical wet-type AMD; 95%CI, 95% confidence intervals; p values were obtained from Fisher's exact text

(GG) risk genotype more often than the non-risk genotype (AA) (typical wet-type AMD cases: p=0.001, OR=6.0; AG and p=2.2×10^{-5}, OR=9.4; GG, PCV cases: p=0.016, OR=3.4; AG and p=0.0002, OR=5.6; GG). A joint OR of 53.5 for typical wet-type AMD in individuals with homozygous (AA and GG) risk alleles at both loci was observed when compared with the non-risk genotype (CC and AA), with a wide range of calculated 95% CI from 7.9 to 361.0. Similarly, a joint OR of 87.4 for PCV in individuals with homozygous (AA and GG) risk alleles at the same loci was observed. A joint analysis of ORs for the rs10490924 and rs2241394 showed that the risk of PCV was 5.4-fold (p=0.017) and 12.8-fold (p=0.0004) if individuals had homozygous (GG) risk genotype of rs2241394 and heterozygous (CA) and homozygous (AA) risk genotype of rs10490924, respectively, compared with the non-risk genotype. A plot of the two-locus genotype specific for typical wet-type AMD and PCV risks further illustrates the stronger impact of rs10490924 on these diseases (Fig. 3).

LD block analyses

rs800292 and rs1061170 are located within exon 2 and exon 9, respectively, of the *CFH* gene on chromosome 1. rs800292 was included in LD block 1 indicated in Fig. 2a. rs1061170 was located in a different LD block from rs800292 (data not shown). The leading two SNPs rs10490924 and rs3750848, which have been reported to associate with AMD [30], maps to a small LD block 1 on chromosome 10 (Fig. 2b). rs10490924 and rs3750848 were located within exon 1 and intron 1 of *ARMS2*. Another SNP, rs2672587, included in the intronic region of *HTRA1* is located downstream of the leading two SNPs between block 1 and 2 (Fig. 2b). rs2230199 and rs2241394 were located within exon3 and intron 13 of the *C3* gene, respectively on chromosome 19. rs2241394 was not included in LD blocks indicated in Fig. 2c.

Discussion

We performed a first genome wide genotyping of Japanese patients with typical wet-type AMD and PCV using Affymetrix GeneChip® Human Mapping 500 K Array and *Taq*Man assay. Previous genome wide scans on individuals with the dry and wet-type AMD in Caucasian populations indicated that *CFH* and *ARMS2/HTRA1* are the two most significantly associated gene regions for AMD

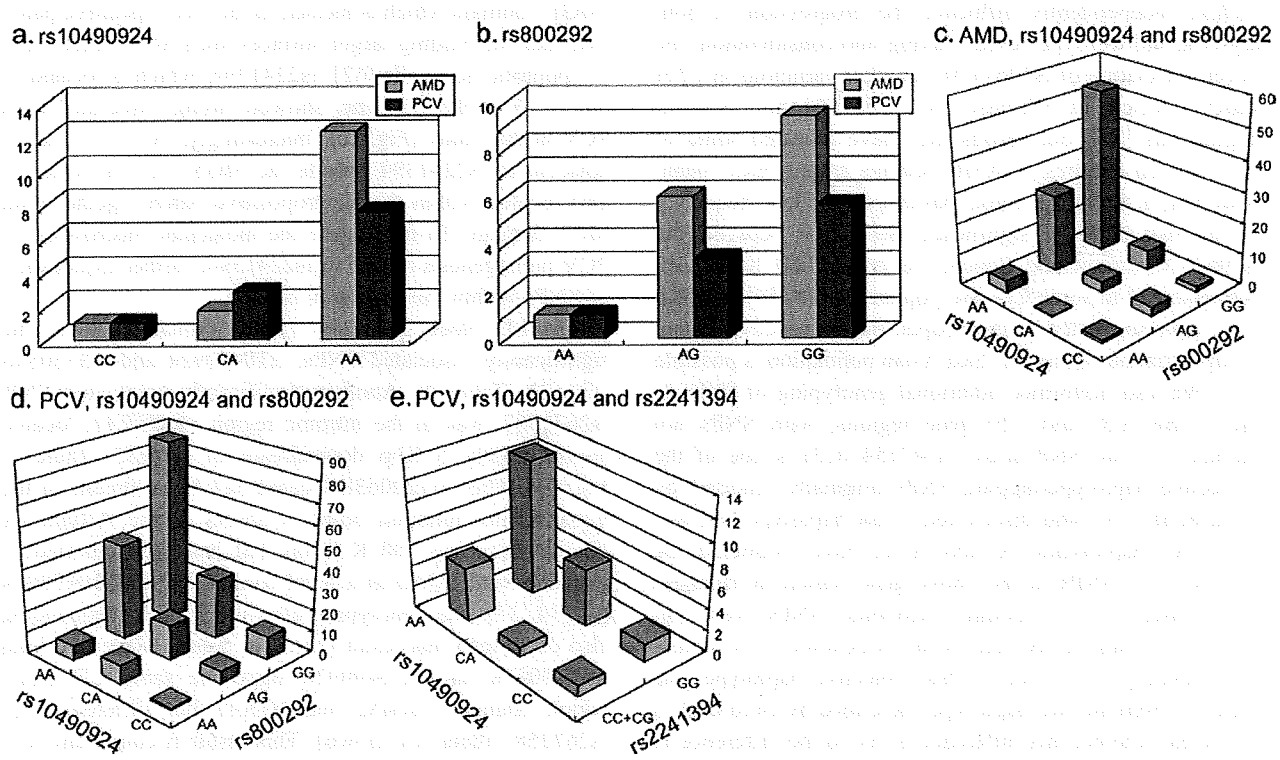

Fig. 3 Schematic view of two-locus odds ratios. *Upper panel*, independently genetic effect of rs10490924 (**a**) and rs800292 (**b**). *Blue boxes*, typical wet-type AMD; *Purple boxes*, PCV. *Down panel*, joint effect of indicated SNPs to typical wet-type AMD and PCV. Joint odds ratios for the combination of rs10490924 and rs800292 for typical wet-type AMD (**c**), rs10490924 and rs800292 for PCV (**d**), and rs10490924 and rs2241394 (**e**) are shown. The combinations had statistically significant odds ratio are *colored*. *AMD* typical wet-type AMD

followed by *C2/BF*, *C3*, and *CFI* [15–18, 26] (Swaroop A, et al. *IOVS* 2009; 50: ARVO E-Abstract 1614). Interestingly, Swaroop et al., reported that the most significantly associated gene locus was *CFH* at p values $<10^{-74}$ followed by *ARMS2* at p values $<10^{-57}$. In contrast, the Japanese typical wet-type AMD patients showed stronger association with *AMRS2/HTRA1* compared to *CFH* (Table 2). Affymetrix GeneChip® Human Mapping 500 K Array used in this study contained 19 SNPs covering the *CFH* gene region (13 SNPs passed the quality control filters). The LD blocks in this region are notably large and with the additional genotyping of rs800292 by *Taq*Man assay, the whole *CFH* gene region has been covered. Thus, the association of rs800292 with typical wet-type AMD and PCV has been confirmed, and the results in this study clearly indicate a lower contribution of *CFH* compared to *AMRS2/HTRA1* on typical wet-type AMD and PCV in the Japanese AMD population. This is consistent with our earlier findings together with others, which have shown lower association of *CFH* compared to *ARMS2/HTRA1* for AMD in Japanese individuals [33, 38–41]. Furthermore, recent studies demonstrated that 10q26 is more strongly associated than 1q32 in wet-type AMD in Caucasian populations [27, 31, 32]. Combining the results of our study with previous studies suggests that *CFH* and *ARMS2/HTRA1* independently influence the progression of both dry-type and wet-type AMD. Taking into consideration, the lower association of rs1061170 and other variations in *CFH* gene reported in Chinese [42, 55, 56] and Korean populations [57], our results may have revealed some of the common features of AMD patients among East Asian. However, it should be noted that despite the low frequency of the risk allele, a significant association between the rs1061170 variant and typical wet-type AMD have been demonstrated in some Chinese population [58, 59]. As Chu et al. have suggested in their paper, the existence of ethnic group variation within the East Asian population is possible [59]. We also performed additional genotyping of SNPs in the *C2/BF*, *C3*, and *CFI* gene regions, with SNPs not included on the SNP array. rs547154 (*C2*) is one of the protective haplotype-tagging SNPs originally reported by Gold et al. [45] who discovered a risk haplotype and two protective haplotypes. Kondo et al. have examined the effects of 11 SNPs in the above gene region in Japanese PCV cases [50]. Although individual SNPs were not associated, statistically significant association of a protective haplotype was found. This protective haplotype was different from the two haplotypes described by Gold et al. It is unclear whether this difference is due to the difference in pathogenesis between dry-type AMD and PCV or ethnicity. As for rs2230199 (*C3*), the risk allele frequency was 0 in subjects analyzed in this study, which was consistent with the data from the Hap Map project. The risk allele for rs2230199 was 0.175 in European population (Hap Map project). In our study, rs2241394 in intron 13 of *C3* gene showed significant association with PCV but not with typical wet-type AMD (Table 2).

The risk of typical wet-type AMD associated with rs10490924 was very high (OR=12.3; 95% CI=6.0–25.3), whereas the risk of PCV conferred by rs10490924 (OR=7.6; 95% CI=3.5–16.1) was similar to the risk of rs800292 (OR=5.6; 95% CI=2.1–15.5) (Table 4). Tam et al. reported that combined rs11200638 and rs800292 caused a 23.3-fold increased risk for exudative AMD [60]. rs11200638 is a SNP shown to be in LD with rs10490924 [29–31]. Similarly, our results showed that the joint risk of rs10490924 and rs800292 for PCV was 87.4-fold (Table 4, Fig. 3).

Structures of CFH and C3 have been reported previously [61, 62]. CFH consists of twenty short consensus repeats, each presumed to fold into a distinct structure termed the complement control protein module (CCP) [61]. Y402H (rs1061170) and I62V (rs800292) are located in the CCP1 and CCP7, which are implicated in C3/C3b binding and polyanion binding, respectively [61]. Accordingly, rs1061170 and rs800292 polymorphisms may differentially influence the CFH activity. C3 consist of multiple domains [62]. R80G (rs2230199) is included in the macroglobulin (MG) 1 domain which is located in the electropositive patch essential for binding target surfaces such as bacterial cells or apoptotic host cells [62]. rs2241394, which is located in intron 13 of the *C3* gene, showed strong associated with PCV in this study (Fig. 2c). Interestingly, exons 13 and 14 adjacent to rs2241394 encode the MG5 domain, which is also located within the electropositive patch together with MG1 domain. To investigate the molecular mechanism of PCV pathogenesis related to rs2241394, further exploration of SNPs within this region is needed.

The LD block including *ARMS2* contains two of the significantly associated SNPs, rs10490924 and rs3750848 (Fig. 2b, Table 2). Another significantly associated SNP, rs2672587, was in the intronic region of *HTRA1*, located approximately 6 Kbp downstream of *ARMS2* (Table 2, Fig. 2b). The rs11200638 located 512 bp upstream of the transcription initiation point is absent in the Affymetrix Human Mapping 500 K Array but has been reported to associate with AMD at a level comparable to rs10490924 [31, 34, 37]. Our genotyping of rs11200638 by sequencing also confirmed this result [33]. Our data indicate that both rs11200638 and rs10490924 share the same LD block which contains *ARMS2* and *HTRA1* but different from rs2672587 (data not shown). This result is consistent with previous Caucasian studies [29–31]. Some of the candidate loci appeared in this study may be specific to the Japanese AMD population or critical for the development of AMD in combination with *ARMS2* (rs10490924) and/or *HTRA1*

(rs11200638), and other behavioral, nutritional, and environmental factors. Further replication and detailed experiments are needed.

Acknowledgments We are grateful to all patients and their families who participated in this study. This study was supported in part by the grant to TI from the National Hospital Organization and the Japanese Ministry of Health, Welfare, and Labour of Japan.

References

1. Ding X, Patel M, Chan CC. Molecular pathology of age-related macular degeneration. Prog Retin Eye Res. 2009;28:1–18.
2. Kawasaki R, Wang JJ, Ji GJ, et al. Prevalence and risk factors for age-related macular degeneration in an adult Japanese population: Funagata study. Ophthalmology. 2008;115:1376–81.
3. Lim JI. Age-related macular degeneration. New York: Marcel Dekker; 2002.
4. Bonilha VL. Age and disease-related structural changes in the retinal pigment epithelium. Clin Ophthalmol. 2008;2:413–24.
5. Maruko I, Iida T, Saito M, et al. Clinical characteristics of exudative age-related macular degeneration in Japanese patients. Am J Ophthalmol. 2007;144:15–22.
6. Gomi F, Tano Y. Popypoidal choroidal vasculopathy and treatments. Curr Opin Ophthalmol. 2008;19:208–12.
7. Cacket P, Wong D, Yeo I. A classification system for polypoidal choroidal vasculopathy. Retina. 2009;29:187–91.
8. Byeon SH, Lee SC, Oh HS, et al. Incidence and clinical patterns of polypoidal choroidal vasculopathy in Korean patients. Jpn J Ophthalmol. 2008;52:57–62.
9. Meyers SM. A twin study on age-related macular degeneration. Trans Am Ophthalmol Soc. 1994;92:775–843.
10. Hammond CJ, Webster AR, Snieder H, et al. Genetic influence on early age-related maculopathy: a twin study. Ophthalmology. 2002;109:730–6.
11. Seddon JM, Cote J, Page WF, et al. The US twin study of age-related macular degeneration: relative roles of genetic and environmental influences. Arch Ophthalmol. 2005;123:321–7.
12. Heiba IM, Elston RC, Klein BE, et al. Sibling correlations and segregation analysis of age-related maculopathy: the Beaver Dam Eye Study. Genet Epidemiol. 1994;11:51–67.
13. Seddon JM, Ajani UA, Mitchell BD. Familial aggregation of age-related maculopathy. Am J Ophthalmol. 1997;123:199–206.
14. Klaver CC, Wolfs RC, Assink JJ, et al. Genetic risk of age-related maculopathy. Population-based familial aggregation study. Arch Ophthalmol. 1998;116:1646–51.
15. Abecasis GR, Yashar BM, Zhao Y, et al. Age-related macular degeneration: a high-resolution genome scan for susceptibility loci in a population enriched for late-stage disease. Am J Hum Genet. 2004;41:482–94.
16. Iyengar SK, Song D, Klein BE, et al. Dissection of genomewide-scan in extended families reveals a major locus and oligogenic susceptibility for age-related macular degeneration. Am J Hum Genet. 2004;74:20–39.
17. Majewski J, Schultz DW, Weleber RG, et al. Age-related macular degeneration—a genome scan in extended families. Am J Hum Gentet. 2003;73:540–50.
18. Seddon JM, Santangelo SL, Book K, et al. A Genomewide scan for age-related macular degeneration provides evidence for linkage to several chromosomal regions. Am J Hum Genet. 2003;73:780–90.
19. Klein ML, Schultz DW, Edwards A, et al. Age-related macular degeneration. Clinical features in a large family and linkage to chromosome 1q. Arch Ophthalmol. 1998;116:1082–8.
20. Schick JH, Iyengar SK, Klein BE, et al. A whole-genome screen of a quantitative trait of age-related maculopathy in sibships from the Beaver Dam Eye Study. Am J Hum Genet. 2003;72:1412–24.
21. Kenealy SJ, Schmidt S, Agarwal A, et al. Linkage analysis for age-related macular degeneration supports a gene on chromosome 10q26. Mol Vis. 2004;10:57–61.
22. Schmidt S, Scott WK, Postel EA, et al. Ordered subset linkage analysis supports a susceptibility locus for age-related macular degeneration on chromosome 16p12. BMC Genet. 2004;5:18.
23. Weeks DE, Conely YP, Tsai HJ, et al. Age-related maculopathy: a genomewide scan with continued evidence of susceptibility loci within the 1q31, 10q26, and 17q25 regions. Am J Hum Genet. 2004;75:174–89.
24. Barral S, Francis PJ, Schultz DW, et al. Expanded genome scan in extended families with age-related macular degeneration. Invest Ophthalmol Vis Sci. 2006;47:5453–9.
25. Fisher SA, Abecasis GR, Yashar BM, et al. Meta-analysis of genome scans of age-related macular degeneration. Hum Mol Genet. 2005;14:2257–64.
26. Edwards AO, Fridley BL, James KM, et al. Evaluation of clustering and genotype distribution for replication in genome wide association studies: the age-related eye disease study. PLoS ONE. 2008;3:e3813.
27. Zhang H, Morrison MA, DeWan A, et al. The NEI/NCBI dbGAP database: genotypes and haplotypes that may specifically predispose to risk of neovascular age-related macular degeneration. BMC Med Genet. 2008;9:51.
28. Klein RJ, Zeiss C, Chew EY, et al. Complement factor H polymorphism in age-related macular degeneration. Science. 2005;308:385–9.
29. Rivera A, Fisher SA, Fritsche LG, et al. Hypothetical ARMS2 is a second major susceptibility gene for age-related macular degeneration, contributing independently of complement factor H to disease risk. Hum Mol Genet. 2005;14:3227–36.
30. Jakobsdottir J, Conley YP, Weeks DE, et al. Susceptibility genes for age-related maculopathy on chromosome 10q26. Am J Hum Genet. 2005;77:389–407.
31. Dewan A, Liu M, Hartman S, et al. HTRA1 promoter polymorphism in wet age-related macular degeneration. Science. 2006;314:989–92.
32. Yang Z, Camp NJ, Sun H, et al. A variant of the HTRA1 gene increases susceptibility to age-related macular degeneration. Science. 2006;314:992–3.
33. Yoshida T, De Wan A, Zhang H, et al. HTRA1 promoter polymorphism predisposes Japanese to age-related macular degeneration. Mol Vis. 2007;13:545–8.
34. Cameron DJ, Yang Z, Chen H, et al. HTRA1 variant confers similar risks to geographic atrophy and neovascular age-related macular degeneration. Cell Cycle. 2007;6:1122–5.
35. Kondo N, Honda S, Ishibashi K, et al. ARMS2/HTRA1 variants in polypoidal choroidal vasculopathy and age-related macular degeneration in a Japanese population. Am J Ophthalmol. 2007;144:608–12.
36. Fuse N, Miyazawa A, Mengkegale M, et al. Polymorphisms in Complement Factor H and Heminectin-1 genes in a Japanese Population with dry-type age-related macular degeneration. Am J Ophthalmol. 2006;142:1074–6.
37. Okamoto H, Umeda S, Obazawa M, et al. Complement factor H polymorphisms in Japanese population with age-related macular degeneration. Mol Vis. 2006;12:156–8.

38. Gotoh N, Yamada R, Hiratani H, et al. No association between complement factor H gene polymorphism and exudative age-related macular degeneration in Japanese. Hum Genet. 2006;120:139–43.
39. Mori K, Gehlbach PL, Kabasawa I, et al. Coding and noncoding variants in the CFH gene and cigarette smoking influence the risk of age-related macular degeneration in a Japanese population. Invest Ophthalmol Vis Sci. 2007;48:5315–9.
40. Uka J, Tamura H, Kobayashi T, et al. No association of complement factor H gene polymorphism and age-related macular degeneration in the Japanese population. Retina. 2006;26:985–7.
41. Grassi MA, Fingert JH, Scheetz TE, et al. Ethnic variation in AMD-associated complement factor H polymorphism p. Tyr402-His. Hum Mutat. 2006;27:921–5.
42. Chen LJ, Liu DT, Tam PO, et al. Association of complement factor H polymorphism with exudative age-related macular degeneration. Mol Vis. 2006;12:1536–42.
43. Lee KY, Vitbana EN, Matbur R, et al. Association analysis of CFH, C2, BF, and HTRA1 gene polymorphisms in Chinese patients with polypoidal choroidal vasculopathy. Invest Ophthalmol Vis Sci. 2008;49:2613–9.
44. Kondo N, Honda S, Kuno S, et al. Coding variant I62V in the complement factor H gene is strongly associated with polypoidal choroidal vasculopahy. Ophthalmology. 2009;116:304–10.
45. Gold B, Merriam JE, Zernant J, et al. Variation in factor B (BF) and complement component 2 (C2) genes is associated with age-related macular degeneration. Nature Genet. 2006;38:458–62.
46. Richardson AJ, Islam FMA, Guymer RH, et al. Analysis of rare variants in the complement component 2 (C2) and factor B (BF) genes refine association for age-related macular degeneration. Invest Ophthalmol Vis Sci. 2009;50:540–3.
47. Maller JB, Fagerness JA, Reynolds RC, et al. Variation in complement factor 3 is associated with risk of age-related macular degeneration. Nature Genet. 2007;39:1200–1.
48. Yates JRW, Sepp T, Matharu BK, et al. Complement C3 variant and the risk of age-related macular degeneration. N Eng J Med. 2009;357:553–61.
49. Fagerness JA, Maller JB, Neale BM, et al. Variation near complement factor I is associated with risk of advanced AMD. Eur J Hum Genet. 2009;17:100–4.
50. Kondo N, Honda S, Kuno S, et al. Role of RDBP and SKIV2L variants in the major histocompatibility complex class III region in polypoidal choroidal vasculopathy etiology. Ophthalmology. 2009;116:1502–9.
51. Seddon JM, Sharma S, Adelman RA. Evaluation of the clinical age-related maculopathy staging system. Ophthalmol. 2006;113:260–6.
52. R Development Core Team. R: A language and environment for statistical computing. Vienna: R Foundation for Statistical Computing; 2009. ISBN 3-900051-07-0, URL http://www.R-project.org.
53. Benjamini Y, Hochberg Y. Controlling the false discovery rate: a practical and powerful approach to multiple testing. J R Stat Soc. 1995;B57:289–300.
54. Agresti A. Categorical Data Analysis. New Jersey: John Wiley & Sons; 2002.
55. Xu Y, Guan N, Xu J, et al. Association of CFH, ARMS2, and HTRA1 polymorphisms with exudative age-related macular degeneration in a northern Chinese population. Mol Vis. 2008;14:1373–81.
56. Ng TK, Chen LJ, Liu DT, et al. Multiple gene polymorphisms in the complement factor h gene are associated with exudative age-related macular degeneration in Chinese. Invest Ophthalmol Vis Sci. 2008;49:3312–7.
57. Kim NR, Kang JH, Kwon OW, et al. Association between complement factor H gene polymorphism and neovascular age-related macular degeneration in Koreans. Invest Ophthalmol Vis Sci. 2008;49:2071–6.
58. Lau LI, Chen SJ, Cheng CY, et al. Association of the Y402H polymorphism in complement factor H gene and neovascular age-related macular degeneration in Chinese patients. Invest Ophthalmol Vis Sci. 2006;47:3242–6.
59. Chu J, Zhou CC, Lu N, et al. Genetic variants in three genes and smoking show strong associations with susceptibility to exudative age-related macular degeneration in a Chinese population. Chin Med J. 2008;121:2525–33.
60. Tam PO, Ng TK, Liu DT, et al. HTRA1 variants in exudative age-related macular degeneration and interactions with smoking and CFH. Invest Ophthalmol Vis Sci. 2008;49:2357–65.
61. Scmidt CQ, Herbert AP, Hocking HG, et al. Translational mini-review series on complement factor H: structural and functional correlations for factor H. Cln Exp Immun. 2008;151:14–24.
62. Janssen BJC, Christodoulidou A, McCarthy A, et al. Structures of C3b reveals conformational changes that underlie complement activity. Nature. 2006;444:213–6.

Letter to the Editor

Stargardt Disease with Preserved Central Vision: identification of a putative novel mutation in ATP-binding cassette transporter gene

Kaoru Fujinami,[1] Masakazu Akahori,[2] Masaki Fukui,[1] Kazushige Tsunoda,[1] Takeshi Iwata,[2] and Yozo Miyake[1,3]

[1]Laboratory of Visual Physiology, National Institute of Sensory Organs, Meguro-ku, Tokyo, Japan
[2]Division of Molecular & Cellular Biology, National Institute of Sensory Organs, National Hospital Organization, Tokyo Medical Center, Meguro-ku, Tokyo, Japan
[3]Aichi Shukutoku University, Aichi, Japan, Nagakute-cho, Aichi-gun, Aichi, Japan

doi: 10.1111/j.1755-3768.2009.01848.x

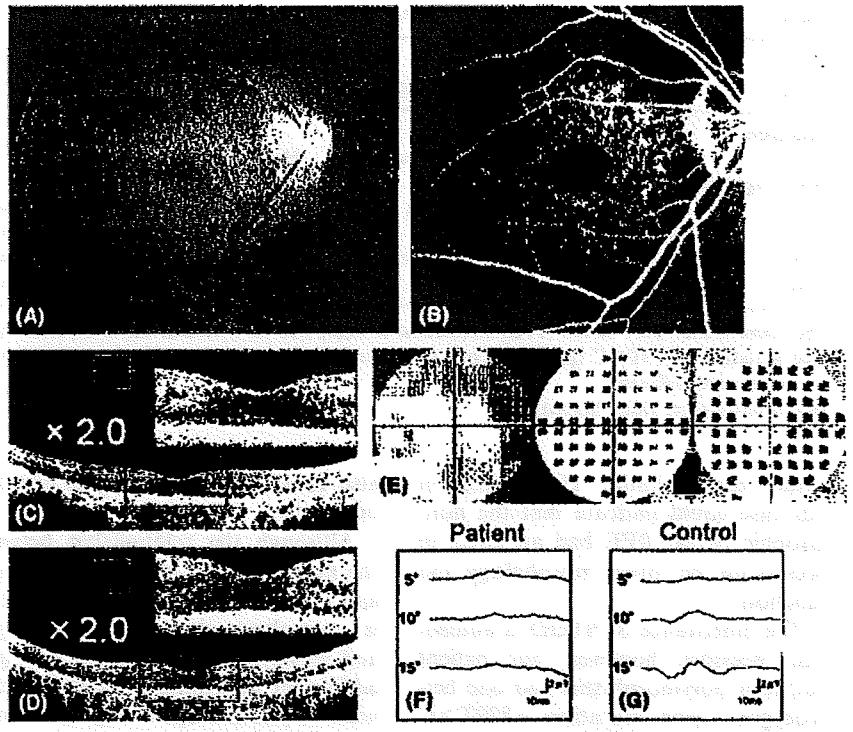

Fig. 1. Fundus photograph (A), fluorescein angiogram (FA) (B), optical coherence tomography (OCT) (C, D), Humphrey static perimetry (E), and focal macular electroretinograms (FMERGs) (F) of an eye of a patient with Stargardt disease. (A) Fundus photograph showing dark brown, well demarcated area in the fovea surrounded by orange-yellow flecks in the macula. (B) FA showing blockage in the foveal area, ring-shaped mottled hyperfluorescence in the macula, and dark choroid. (C, D) OCT images (C: horizontal, D: vertical) showing well-preserved sensory retina and retinal pigment epithelium (RPE) layer in the fovea. In the juxtafoveal region, an atrophy of both sensory retina and RPE can be seen. The enlarged images within the red lines are attached. (E) Humphrey static perimetry showing ring-shaped paracentral relative scotoma (10-2 strategy). (F, G) FMERGs showing normal responses elicited by a 5-degree stimulus spot and severely reduced responses elicited by 10-degree and 15-degree spots, when compared with the age-matched control.

Editor,

Stargardt disease (STGD) has a juvenile to young-adult onset, a rapid decrease of central vision and a progressive bilateral atrophy of the sensory retina and retinal pigment epithelium (RPE) in the macula. Yellow-orange flecks are often detected around the macula, the midretina and or both (Rotenstreich et al. 2003). Mutations in the gene encoding the ATP-binding cassette transporter gene (ABCA4) are responsible for autosomal recessive STGD (Allikmets 1997; Webster et al. 2001). We examined a patient who had the characteristic signs of STGD but had good visual acuity.

A 66-year-old man complained of photophobia and a paracentral scotoma which was present since his teens and had not worsened. None of his family members had similar symptoms. His visual acuity was 20/15 OU, and ophthalmoscopy identified a dark brown, well-demarcated area at the fovea surrounded by RPE atrophy and flecks (Fig. 1A). Fluorescein angiography showed window defects at the flecks and a dark choroid (Fig. 1B). The optical coherence tomographic (OCT) images showed a well-preserved sensory retina and normal thickness RPE at the fovea (Fig. 1C, D). The foveal area was surrounded by atrophic sensory retina and RPE. Static perimetry showed ring-shaped paracentral relative scotoma which surrounded the normal area seeing area of 5° (Fig. 1E). Focal macular electroretinograms (FMERGs) also demonstrated a well-preserved retinal function at the fovea (Fig. 1F). Compared to age-matched controls, the FMERGs had normal responses elicited by a 5-degree stimulus spot and severely reduced responses elicited by 10-degree and 15-degree spots (Fig. 1F, G). Genetic analysis with direct DNA sequencing of amplified products revealed four reported polymorphisms (Allikmets 1997; Briggs et al. 2001; Webster et al. 2001; Fukui et al. 2002) and one novel mutation, Met280Thr, in exon 7 of the ABCA4 gene (Table 1).

Our patient had clinical findings that were pathognomonic of typical STGD, except that the clinical course was stationary and he had 20/15 vision because of well-preserved foveal function. The preserved foveal area was small and well demarcated. Visual acuity, fundus appearance, OCT images, static perimetry and FMERGs supported the well-preserved foveal function. We report our case because the patient had a unique phenotype with a novel putative mutation in the *ABCA4* gene, not yet shown to segregate with the disease.

The well-demarcated dark brown foveal RPE appeared to be hyperpigmented although the thickness measured by OCT was 29 μm which was

Table 1. ABCA4 GENE MUTATION AND Polymorphisms.

Exon	Nucleotide Change	Effect Changes	Het/Hom	References
Mutation				
7	c.839T > C	p.Met280Thr	Het	Present study
Polymorphisms				
10	c.1269C > T	p.His424His	Hom	Webster AR et al.
45	c.6249C > T	p.Ile2083Ile	Het	Allikmets R et al.
46	c.6285T > C	p.Asp2095Asp	Het	Briggs CE et al.
49	c.6764G > T	p.Ser2255Ile	Het	Allikmets R et al.

The translational start codon ATG/methionine is numbered as +1. One novel disease-associated mutation [c.839T > C (p.Met280Thr)] was found. References of previously reported polymorphisms are indicated.
Het, heterozygote; Hom, homozygote.

within normal limits. The findings in our case could indicate that the non-atrophic foveal RPE had an effect in preserving the foveal morphology and function.

The inheritance of STGD is autosomal recessive; however, our patient had four polymorphisms and one heterozygous gene mutation c.839T > C in exon 7 in the *ABCA4* gene. A second mutation was not found, but it may well exist outside of the coding sequence of the *ABCA4* gene. The new mutation in our patient was located outside the known functional domains of ATP-binding or transmembrane site (Lewis et al. 1999), which may explain the mild effect of the missense mutation. We should also consider a modifier gene effect in our patient.

Although the relationship between the new mutation of the *ABCA4* gene and the well-preserved foveal structure is unresolved, the unique phenotype and genotype of our patient may give additional information on the mechanism of photoreceptor degeneration in eyes with STGD.

References

Allikmets R (1997): A photoreceptor cell-specific ATP-binding transporter gene (ABCR) is mutated in recessive Stargardt macular dystrophy. Nat Genet 17: 122.

Briggs CE, Rucinski D, Rosenfeld PJ, Hirose T, Berson EL & Dryja TP (2001): Mutations in ABCR (ABCA4) in patients with Stargardt macular degeneration or cone-rod degeneration. Invest Ophthalmol Vis Sci 42: 2229–2236.

Fukui T, Yamamoto S, Nakano K et al. (2002): ABCA4 gene mutations in Japanese patients with Stargardt disease and retinitis pigmentosa. Invest Ophthalmol Vis Sci 43: 2819–2824.

Lewis RA, Shroyer NF, Singh N et al. (1999): Genotype/Phenotype analysis of a photoreceptor-specific ATP-binding cassette transporter gene, ABCR, in Stargardt disease. Am J Hum Genet 64: 422–434.

Rotenstreich Y, Fishman GA & Anderson RJ (2003): Visual acuity loss and clinical observations in a large series of patients with Stargardt disease. Ophthalmology 110: 1151–1158.

Webster AR, Heon E, Lotery AJ et al. (2001): An analysis of allelic variation in the ABCA4 gene. Invest Ophthalmol Vis Sci 42: 1179–1189.

Correspondence:
Kazushige Tsunoda, MD
Laboratory of Visual Physiology
National Institute of Sensory Organs
2-5-1 Higashigaoka
Meguro-ku
Tokyo 152-8902
Japan
Tel: + 81 3 3411 0111 ext. 6615
Fax: + 81 3 3412 9811
Email: tsunodakazushige@kankakuki.go.jp

OPEN ACCESS Freely available online

PLoS one

VAV2 and *VAV3* as Candidate Disease Genes for Spontaneous Glaucoma in Mice and Humans

Keiko Fujikawa[1,3,6]*, Takeshi Iwata[2], Kaoru Inoue[3], Masakazu Akahori[2], Hanako Kadotani[1], Masahiro Fukaya[4], Masahiko Watanabe[4], Qing Chang[5], Edward M. Barnett[5], Wojciech Swat[6]

1 Department of Pathology and Immunology, Hokkaido University Graduate School of Medicine, Sapporo, Japan, **2** National Institute of Sensory Organs, National Hospital Organization Tokyo Medical Center, Tokyo, Japan, **3** Faculty of Health Science, Hokkaido University, Sapporo, Japan, **4** Department of Anatomy, Hokkaido University Graduate School of Medicine, Sapporo, Japan, **5** Department of Ophthalmology and Visual Sciences, Washington University School of Medicine, St. Louis, Missouri, United States of America, **6** Department of Pathology and Immunology, Washington University School of Medicine, St. Louis, Missouri, United States of America

Abstract

Background: Glaucoma is a leading cause of blindness worldwide. Nonetheless, the mechanism of its pathogenesis has not been well-elucidated, particularly at the molecular level, because of insufficient availability of experimental genetic animal models.

Methodology/Principal Findings: Here we demonstrate that deficiency of Vav2 and Vav3, guanine nucleotides exchange factors for Rho guanosine triphosphatases, leads to an ocular phenotype similar to human glaucoma. Vav2/Vav3-deficient mice, and to a lesser degree Vav2-deficient mice, show early onset of iridocorneal angle changes and elevated intraocular pressure, with subsequent selective loss of retinal ganglion cells and optic nerve head cupping, which are the hallmarks of glaucoma. The expression of Vav2 and Vav3 tissues was demonstrated in the iridocorneal angle and retina in both mouse and human eyes. In addition, a genome-wide association study screening glaucoma susceptibility loci using single nucleotide polymorphisms analysis identified *VAV2* and *VAV3* as candidates for associated genes in Japanese open-angle glaucoma patients.

Conclusions/Significance: Vav2/Vav3-deficient mice should serve not only as a useful murine model of spontaneous glaucoma, but may also provide a valuable tool in understanding of the pathogenesis of glaucoma in humans, particularly the determinants of altered aqueous outflow and subsequent elevated intraocular pressure.

Citation: Fujikawa K, Iwata T, Inoue K, Akahori M, Kadotani H, et al. (2010) *VAV2* and *VAV3* as Candidate Disease Genes for Spontaneous Glaucoma in Mice and Humans. PLoS ONE 5(2): e9050. doi:10.1371/journal.pone.0009050

Editor: Patrick Callaerts, Katholieke Universiteit Leuven, Belgium

Received January 22, 2009; **Accepted** January 18, 2010; **Published** February 4, 2010

Funding: The work described in this report was funded in parts by a grant from the Ministry of Education, Culture, Sports, Science and Technology in Japan. The funders had no role in study design, data collection and analysis, decision to publish, or preparation of the manuscript.

Competing Interests: The authors have declared that no competing interests exist.

* E-mail: fujikawa@med.hokudai.ac.jp

Introduction

The critical importance of elevated intraocular pressure (IOP) in the pathogenesis of glaucomatous optic neuropathy is widely recognized [1,2]. While compromise of aqueous humor outflow is the key determinant of elevation in IOP [3,4], the molecular mechanisms underlying changes in the outflow pathway that lead to elevated IOP remain to be elucidated. For this reason, mouse genetic knockout models of spontaneous glaucoma are highly sought after.

The Vav proteins are the best-characterized family of guanine nucleotide exchange factors (GEFs) that activates Rho guanosine triphosphatases (GTPases) in a phosphorylation-dependent manner [5]. Rho GTPases control cell behavior via regulating the specific filamentous actin structures involved in migration, adhesion, and morphogenesis, by acting as binary switches cycling between an inactive (GDP-bound) and active (GTP-bound) state [6]. The three mammalian Vav proteins, Vav1, Vav2, and Vav3, share a Dbl homology domain for their enzymatic activity as GEFs and contain a common structural array characteristic of proteins involved in signal transduction. Regardless of the structural similarity, Vav proteins differ in their tissue distribution. Vav1 is expressed specifically in lymphoid lineage cells, whereas Vav2 and Vav3 are more widely expressed [5,7]. Genetic approaches using knockout mice have provided valuable information on the function of Vav proteins *in vivo*. Vav proteins are crucial for the development and function of hematopoietic lineage cells such as lymphocytes, neutrophils, natural killer cells, and osteoclasts [8–16]. Individual Vav proteins exhibit both redundant and specialized functions. Despite the wide distribution of Vav2 and Vav3 proteins in mouse tissues, little is known about their specific function in non-hematopoietic cells.

While trying to better elucidate the functions of Vav2 and Vav3 in non-hematopoietic cells, we discovered that Vav2/Vav3-deficient mice have a significant ocular phenotype. Specifically, we show that Vav2/Vav3-deficient mice have elevated IOP, which eventually manifests as buphthalmos. Loss of Vav2 and Vav3 expression is associated with changes in the iridocorneal angle, with eventual chronic angle closure. The elevation of IOP in Vav2/Vav3-deficient mice is accompanied by an optic

neuropathy characterized by selective loss of retinal ganglion cells (RGCs) and optic nerve head (ONH) excavation and is therefore consistent with glaucoma. In addition, both *VAV2* and *VAV3* are shown to be susceptibility loci by single nucleotide polymorphisms (SNPs) study of Japanese primary open-angle glaucoma patients.

Results

Vav2/Vav3-Deficient Mice Develop Buphthalmos

Eyes of Vav2/Vav3-deficient ($Vav2^{-/-}Vav3^{-/-}$) mice were noted to develop buphthalmos starting between 6 and 12 weeks of age (Figure 1). This enlargement was typically seen unilaterally at first, with frequent bilateral involvement over the next 1–2 months, and continued enlargement until the mice were 6-months old. Eventually, some of the eyes, became atrophic and phthisical in appearance (Figure 1A). In order to confirm our initial observations, we measured the corneal diameters and weights of $Vav2^{-/-}Vav3^{-/-}$ mice eyes and compared them with age-matched wild-type mice eyes (Figure 1B). The examination clearly showed our observations were relevant. We observed 200 $Vav2^{-/-}Vav3^{-/-}$ mice at 6 months of age and almost 75% of them showed the enlarged eyes (Figure 1C). In addition, histological study indicated that there were no abnormal findings in the tissues both around the enlarged eyes such as inflammation, tumor, or hyperplasia, and in the thyroid of the $Vav2^{-/-}Vav3^{-/-}$ mice (data not shown).

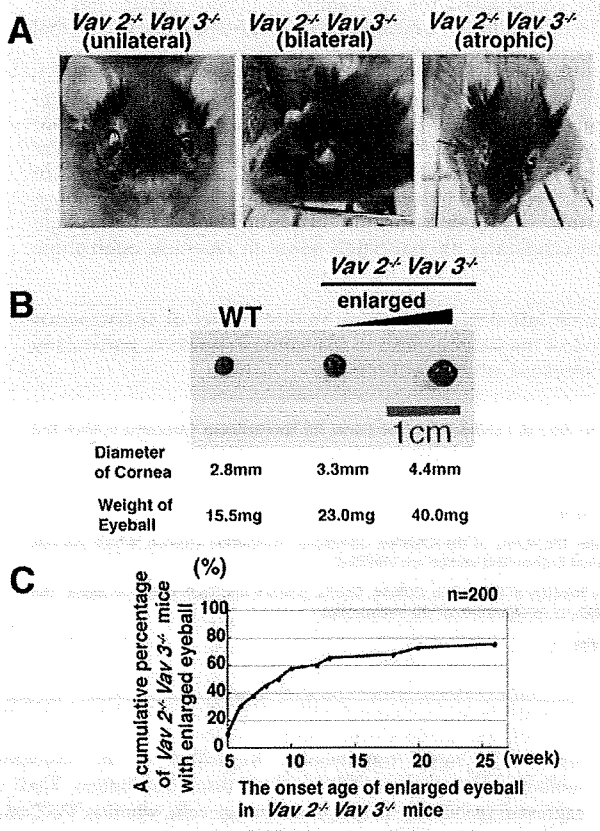

Figure 1. Vav2/Vav3-deficient mice develop buphthalmos. Eyes of Vav2/Vav3-deficient ($Vav2^{-/-}Vav3^{-/-}$) mice develop buphthalmos between 6 and 12 weeks of age. **A.** Left photo: Representative photo of unilateral enlarged eye in 10-week-old $Vav2^{-/-}Vav3^{-/-}$ mice. Centre photo: Representative photo of bilateral enlarged eyes in 16-week-old $Vav2^{-/-}Vav3^{-/-}$ mice. Right photo: Representative photo of enlarged eye becoming atrophic in 8-week-old $Vav2^{-/-}Vav3^{-/-}$ mice. **B.** Comparison of eye sizes. Left panel: Representative eye of 10-week-old wild-type (WT) mice as a control (n = 20). Cornea diameter is 2.9±0.1 mm. Weight is 15.8±1.1 mg. Centre panel: Representative first-recognized enlarged eye of $Vav2^{-/-}Vav3^{-/-}$ mice (9- to 10-week-old, n = 20). The cornea diameter is 3.3±0.1 mm. Weight is 23.7±4.4 mg. $P<0.001$. Right panel: Representative moderately enlarged eye of 12-week-old $Vav2^{-/-}Vav3^{-/-}$mice (n = 20). The cornea diameter is 4.2±0.4 mm. Weight is 38.0±4.0 mg. **C.** Age of onset of enlarged eyes up to 25 weeks of age in $Vav2^{-/-}Vav3^{-/-}$ mice (n = 200). The vertical axis is a cumulative percentage of $Vav2^{-/-}Vav3^{-/-}$ mice with enlargement of the eyes.
doi:10.1371/journal.pone.0009050.g001

Elevation of Intraocular Pressure of Vav-Deficient Mice

As we observed the development of buphthalmos, we assessed for elevated IOP in $Vav2^{-/-}Vav3^{-/-}$, Vav2-deficient ($Vav2^{-/-}$), and Vav3-deficient ($Vav3^{-/-}$) mice. IOP was measured using a rodent tonometer (Tonolab) starting at 4 weeks post-natal and were compared with age-matched wild-type C57BL/6 mice. Reliable measurement of IOP before 4 weeks of age was not possible. At 6 weeks of age, $Vav2^{-/-}Vav3^{-/-}$ mice first showed increased IOP (18.2±3.1 vs. 14.0±2.4 mmHg, $p<0.05$), with further increases out to 10 weeks of age (22.5±7.4 vs. 14.6±4.2 mmHg, $p<0.01$) (Figure 2A). IOP measurements in $Vav2^{-/-}Vav3^{-/-}$ mice ranged from 11–40 mmHg between 7 weeks and 16 weeks of age. There was a statistically significant difference in IOP between the $Vav2^{-/-}Vav3^{-/-}$ and wild-type mice at all time points demonstrated. The phenotype of littermate wild type mice was identical to that of the "inbred" C57BL/6 strain (Figure S1).

In $Vav2^{-/-}$ mice, elevated IOP was first detected at 7 weeks of age. The IOP for $Vav2^{-/-}$ mice was found to be increased at 8 weeks of age compared to wild-type mice (15.5±3.7 vs. 14.0±4.2 mmHg, $p<0.05$)(Figure 2B). The IOP of $Vav2^{-/-}$ mice showed further increases at 10 weeks of age (18.1±3.7 vs. 14.6±4.2 mmHg, $p<0.01$) and remained significantly higher at 12 weeks. In contrast, the IOP of $Vav3^{-/-}$ mice did not differ significantly from wild-type mice between 8 and 12 weeks (Figure 2C). The phenotype of littermate wild type mice was identical to that of inbred strain "C57BL/6". We also demonstrated that the phenotype of Vav2 and Vav3 heterozygous littermate mice ($Vav2^{+/-}$, and $Vav3^{+/-}$) were same as that of wild type (Figure S1).

Retinal Ganglion Cell Loss and Optic Nerve Head Changes in Vav2/Vav3-Deficient Mice

We next examined whether Vav2/Vav3-deficient ($Vav2^{-/-}Vav3^{-/-}$) mice showed changes in the retinal ganglion cell (RGC) layer and optic nerve head (ONH). At 3 weeks of age, $Vav2^{-/-}Vav3^{-/-}$ mice did not show any histological difference in the ONH or the number of RGCs compared to that of age-matched wild-type mice (Figure 3A). At 10 weeks of age, following several weeks of IOP elevation, early signs of ONH cupping and cell body loss in the RGC layer were apparent in $Vav2^{-/-}Vav3^{-/-}$ mice (Figure 3B). At 15 and 30 weeks of age, $Vav2^{-/-}Vav3^{-/-}$ mice showed further evidence of ONH cupping and RGC loss in the context of an otherwise normal retinal architecture. These findings are consistent with a selective loss of RGCs with corresponding changes in the ONH, which are the hallmarks of glaucoma.

Iridocorneal Angle Histopathology in Vav-Deficient Mice

As histopathological examination of globes from mice with buphthalmos frequently demonstrated angle closure, we compared

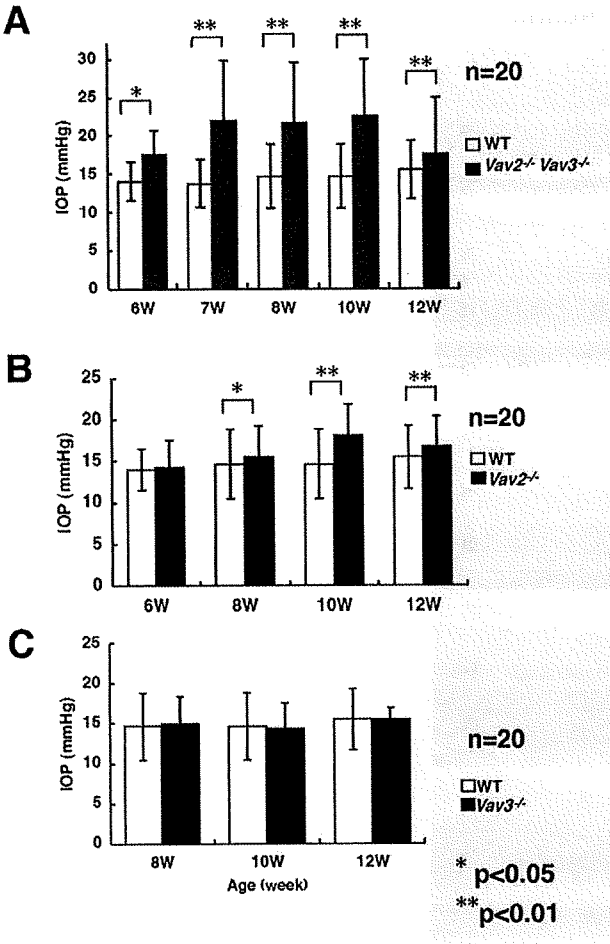

Figure 2. Elevated intraocular pressure of $Vav2^{-/-}Vav3^{-/-}$ and $Vav2^{-/-}$ mice. The intraocular pressure (IOP) of Vav2/Vav3-deficient ($Vav2^{-/-}Vav3^{-/-}$), Vav2-deficient ($Vav2^{-/-}$), and Vav3-deficient ($Vav3^{-/-}$) mice were measured between 10–12 AM. At the indicated ages, twenty mice were examined, respectively. For the IOP measurement of each Vav-deficient mouse, IOP of an age-matched wild-type (WT) mouse was also measured under the same conditions. We confirmed that these results were reproducible with four independent examinations. **A.** IOPs of $Vav2^{-/-}Vav3^{-/-}$ mice were dramatically elevated at 6 weeks of age. **B.** $Vav2^{-/-}$ mice also showed elevated IOP from around 8 weeks of age. **C.** $Vav3^{-/-}$ mice have normal range of IOP at any age. Error bars represent S.D. *P<0.05, **P<0.01 versus WT mice.
doi:10.1371/journal.pone.0009050.g002

the iridocorneal angle histology of 20 Vav2/Vav3-deficient ($Vav2^{-/-}Vav3^{-/-}$) mice with wild-type mice at both 7 and 12 weeks of age. Angles were classified as either being completely open, displaying evidence of partial occlusion of the trabecular meshwork (TM) as manifest by peripheral anterior synechiae (PAS), or being completely closed (total occlusion of the trabecular meshwork)(Figure 4A). Over half of the Vav2/Vav3-deficient mice already showed evidence of angle closure by 7 weeks of age, increasing to nearly 80% in 12-week-old mice (Figure 4B).

We also examined the correlation between elevated IOP and angle changes in 7-week-old $Vav2^{-/-}Vav3^{-/-}$ mice respectively (n = 20) (Figure S2). The mean and standard deviation of IOP in 7-week-old wild-type mice (n = 18) were 13.7±3.12 mmHg respectively. The 95th percentile of those IOPs using a normal curve was 18.8 mmHg. So that IOP over 18.8 mmHg was regarded as elevated IOP. $Vav2^{-/-}Vav3^{-/-}$ mice with elevated IOP showed evidence of angle closure by histological analysis, while $Vav2^{-/-}Vav3^{-/-}$ mice with non-elevated IOP displayed either open angles or evidence of early angle closure (PAS) and angle closure.

In addition, to characterize the progression of angle changes, two additional time points were added to this analysis of the iridocorneal angle −18 days and 4 weeks of age (n = 20 each). While at 18 days of age nearly half of the eyes demonstrated open angles, a large percentage already showed evidence of PAS (Figure 4B). By 4 weeks of age, $Vav2^{-/-}Vav3^{-/-}$ mice showed increasing frequencies of both PAS and angle closure. Taken as a whole, the data showed a gradual progression from open angles to PAS formation to closed angle from 18 days to 12 weeks.

The iridocorneal angles of Vav2-deficient ($Vav2^{-/-}$) and Vav3-deficient ($Vav3^{-/-}$) mice were examined histologically and graded in a similar manner. The iridocorneal angles of $Vav2^{-/-}$ mice also demonstrated evidence of progressive angle closure, but to a lesser extent as compared with $Vav2^{-/-}Vav3^{-/-}$ mice (Figure 4B). $Vav3^{-/-}$ mice had normal appearing open angles without evidence of PAS formation or angle closure (Figure 4B).

In order to better investigate the status of iridocorneal angles in $Vav2^{-/-}Vav3^{-/-}$ mice, we stained for myocilin as a marker for TM cells, as myocilin is strongly expressed in TM cells [17]. We examined 7-week-old $Vav2^{-/-}Vav3^{-/-}$ mice with non-elevated IOP who had either open angles or who displayed evidence of angle closure. As shown in Figure S3, myocilin was not detected in the iridocorneal angle of $Vav2^{-/-}Vav3^{-/-}$ mice with angle closure, but was seen in mice with open angles similar to those of wild-type mice.

Effects of Ocular Hypotensives in Vav2/Vav3 -Deficient Mice

We next tested the efficacy of ocular hypotensives used for human glaucoma in $Vav2^{-/-}Vav3^{-/-}$ mice with elevated IOP (Figure S4). The elevated IOP of 7-week-old $Vav2^{-/-}Vav3^{-/-}$ mice was dramatically reduced by ocular hypotensives used in humans, such as latanoprost, a prostaglandin analogue (Figure S4A). We also tested the IOP-lowering effect in $Vav2^{-/-}Vav3^{-/-}$ mice by two other ocular hypotensives, dorzolamide and timolol, whose mechanisms of action differ from that of latanoprost [18–20], being aqueous suppressants (Figure S4B). Furthermore, we tested Y-27632, a Rho-associated protein kinase inhibitor, that has been reported to cause a reduction in IOP presumably by altering cellular behavior of TM cells [21–23]. Y-27632 showed no effect of lowering IOPs against $Vav2^{-/-}Vav3^{-/-}$ mice, while it lowered the IOP significantly in age-matched wild-type mice (Figure S4C).

Expression of Vav2 and Vav3 in Mouse and Human Eyes

In order to understand the pathogenesis of the Vav2/Vav3-deficient eye phenotype, we examined the mRNA and protein expression patterns of Vav2 and Vav3 in the eye (Figure 5). Quantitative real-time PCR revealed that Vav2 and Vav3 mRNA are expressed in TM, cornea, retina, lens, iris, and ciliary body in the mouse eye (Figure 5A). Vav3 mRNA was more abundantly expressed than that of Vav2 in the TM and the retina. Gene expression levels of both Vav2 and Vav3 in the eye were comparable to levels found in immune cells where Vavs play a critical role [5,7–16]. Next, the Vav2 and Vav3 mRNA localization in mouse eye was examined by in situ hybridization (ISH) analysis (Figure 5B). Both Vav2 and Vav3 oligo probes (antisense), we used here, have been examined the specificities before and proved to have its specificity. As negative controls for

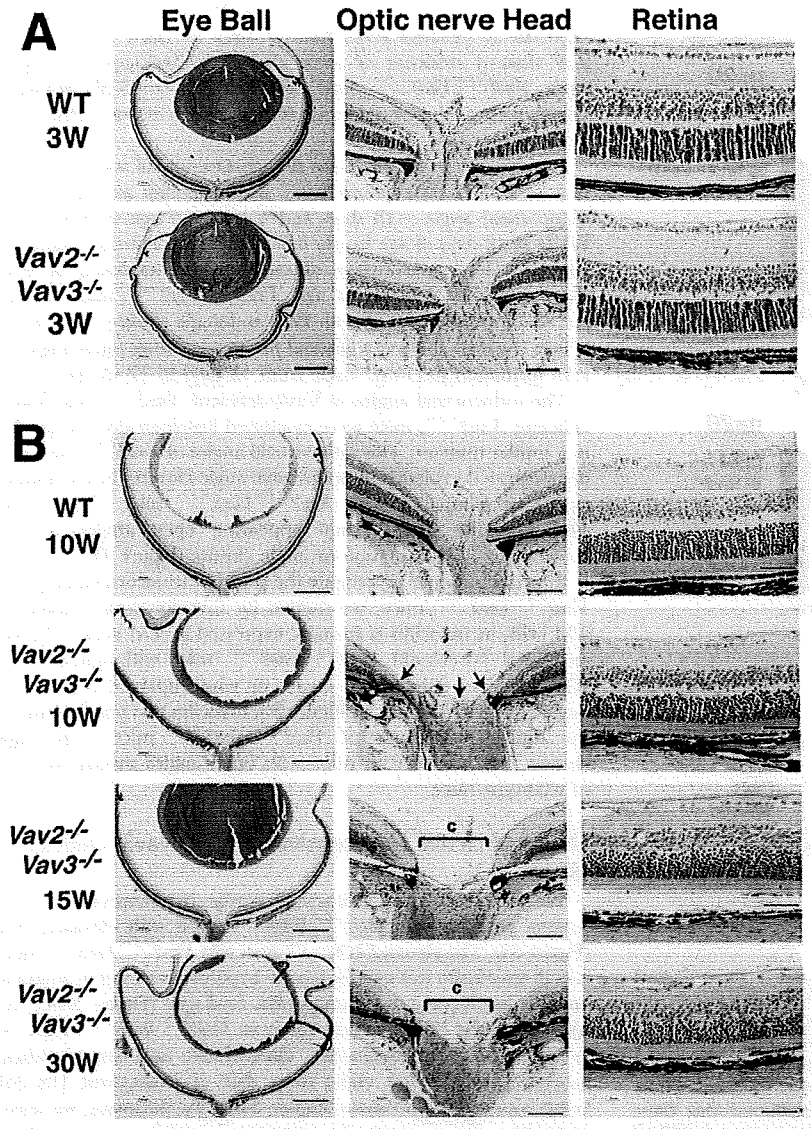

Figure 3. Optic nerve head degeneration and decrease in RGCs observed in *Vav2*$^{-/-}$*Vav3*$^{-/-}$ mice with elevated IOP. Light-microscopic histological examination is conducted to evaluate retinal neuropathy in Vav2/Vav3-deficient (*Vav2*$^{-/-}$*Vav3*$^{-/-}$) mice. **A.** At the age of 3 weeks, *Vav2*$^{-/-}$ *Vav3*$^{-/-}$ mice exhibited impairment of angle status, but no abnormal findings of Optic nerve head degeneration (ONH) or retinal ganglion cells (RGCs) in the retinas. Scale bars, from left to right side: 500 μm, 100 μm, and 50 μm. **B.** After elevation of IOP, compared to control wild-type (WT) mice in the upper panel, ONH in 10-, 15-, and 30-week-old *Vav2*$^{-/-}$*Vav3*$^{-/-}$ mice present so-called capping (shown in c) and thin retinal neural layers (indicated by arrows in the photos). In those retinas, RGCs are decreased. Scale bars, from left to right side: 500 μm, 100 μm, and 50 μm. Sections are representative from 6–12 samples.
doi:10.1371/journal.pone.0009050.g003

these experiments, we used sense probes of Vav2 and Vav3, respectively, which showed no detectable signal (Figure S5). Both genes expression were widely distributed in the ocular tissues including the iridocorneal angle, retina, cornea, and sclera. The co- localization of Vav2 and Vav3 mRNA expression in iridocorneal angle, such as TM, was confirmed by ISH. Also, we assessed Vav2 and Vav3 protein expression by immunoblotting in both mouse and human eyes (Figure 5C). In mouse eyes, expression of both Vav2 and Vav3 was demonstrated in several ocular tissues including the iridocorneal angle, retina, cornea, and sclera. Both Vav2 and Vav3 proteins were also expressed in human retina and iridocorneal angle. The migrated bands were absent in the liver extracts of the *Vav2*$^{-/-}$*Vav3*$^{-/-}$ mice. Results of densitometric ratio (Vav3/Vav2) from normalized protein loading in each lane revealed that Vav3 was more abundantly expressed than Vav2 in the iridocorneal angle tissues of both mouse and human eyes and also in the retina.

Single Nucleotide Polymorphisms in Japanese Primary Open-Angle Glaucoma Patients

We observed Vav2 and Vav3 proteins expression in the tissues of human iridocorneal angle and retina. In order to investigate the

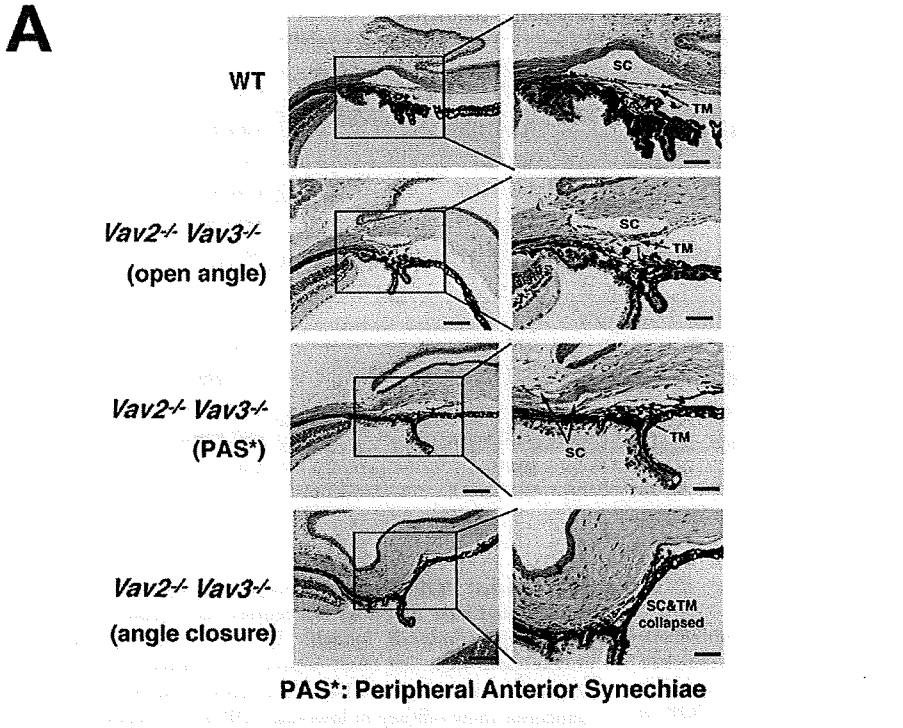

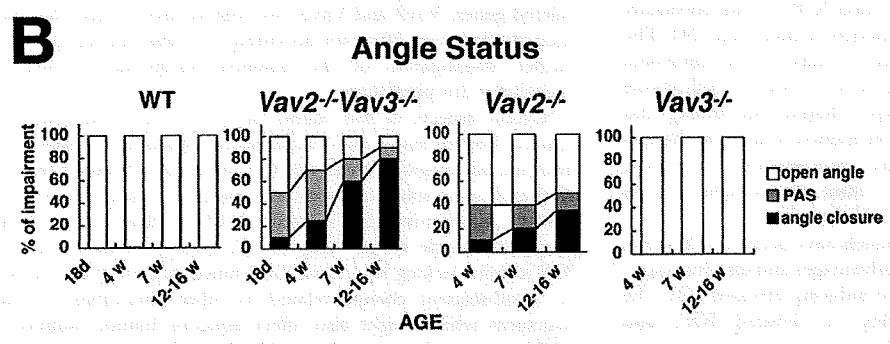

Figure 4. Characterization of progressive iridocorneal angle closures in $Vav2^{-/-}Vav3^{-/-}$ and $Vav2^{-/-}$ mice. The aqueous humor outflow facility, trabecular meshwork (TM) and Schlemm's canal (SC) (iridocornial angle) in Vav2/Vav3-deficient ($Vav2^{-/-}Vav3^{-/-}$) mice are evaluated in histological manner. Vav2-deficient ($Vav2^{-/-}$) mice also have the same changes, but of lower severity. **A.** Representative photos of normal TM and SC histology of 12-week-old wild-type (WT) mice as a control. Representative photos of normal open angle, peripheral anterior synechiae (PAS) in 12-week-old $Vav2^{-/-}Vav3^{-/-}$ mice, and angle closure status in 12-week-old $Vav2^{-/-}Vav3^{-/-}$ mice. Sections used here are all representative from 20 samples. Scale bars: left photos, 200 μm; right photos, 100 μm. **B.** Changes of angle status appear at the early ages. We classify angle status of $Vav2^{-/-}$ $Vav3^{-/-}$, $Vav2^{-/-}$, and $Vav3^{-/-}$mice into open angle, PAS, and angle closure by histological evaluation. We find the changes of angle status at the early ages, such as in 18-day-old $Vav2^{-/-}Vav3^{-/-}$ *mice* (n = 20) and in 4-week-old of $Vav2^{-/-}Vav3^{-/-}$ *mice* (n = 20). We took four ($Vav2^{-/-}Vav3^{-/-}$) and three ($Vav2^{-/-}$, $Vav3^{-/-}$) different age groups, with 20 mice examined, respectively.
doi:10.1371/journal.pone.0009050.g004

relevant association of *VAV2* and *VAV3* in human glaucoma patients, we carried out a genome-wide association study using the Affymetrix GeneChip Human Mapping 500 K Array Set. We examined Japanese primary open–angle glaucoma (POAG) cases and age-matched non-glaucoma controls. Both *VAV2* and *VAV3* loci in Japanese POAG patients showed SNPs against the non-glaucoma controls for dbSNPs rs2156323 and rs2801219, respectively. We reported the most extreme (Table 1). Both were intronic SNPs, SNP rs2156323 lying in intron3 of *VAV2* and SNP rs2801219 lying in intron1 of *VAV3*. *VAV2* SNP rs2156323 in particular indicated significant association with Japanese POAG, including a 5.65 heterozygote odds ratio (95% confidence interval (CI): 1.99–16.0), 4.34 heterozygote relative risk (95% CI: 1.72–10.44) and 4.38×10^{-4} genotypic *P* value with respect to risk allele A.

Judging from alleric *P*-values distribution for detecting *VAV2* ranking and genotypic *P*- values distribution for *VAV3* ranking, we observed that *VAV2* and *VAV3* showed high scores ($-\log_{10}(P)$) among approximately 380,000 SNPs analyzed in this study (Figure 6). On the contrary, *VAV1* showed no association with the POAG. These data strongly suggest that *VAV2* and *VAV3* genes are susceptibility loci in Japanese POAG.

Table 1. Vav2, Vav3, Vav1 association study for POAG using the Affymetrix GeneChip.

Gene	*VAV2*	*VAV3*	*VAV1*
SNP ID	rs2156323	rs2801219	rs2617815
Chromosome Location	9q34.1	1p13.3	19p13.2
Position	133750375	108214454	6746147
Genotypic *P* value	4.38×10^{-4}	5.42×10^{-4}	4.41×10^{-2}
Allele	AG	AC	AG
Risk allele	A	C	G
Minor allele	A	C	G
Heterozygote odds ratio (95%CI)	5.65 (1.99–16.0)	2.03 (1.01–4.09)	1.04 (0.52–2.08)
Heterozygote relative risk (95%CI)	4.34 (1.72–10.44)	1.31 (1.00–1.75)	1.01 (0.82–1.23)
Homozygote odds ratio	Not Available	Not Available	Not Available
Exon Intron	*VAV2* Intron3	*VAV3* Intron1	*VAV1* Intron1
SNP type	iSNP*1	iSNP	iSNP

*1: intronic S.

doi:10.1371/journal.pone.0009050.t001

Discussion

To our knowledge, this is the first report of a spontaneous glaucoma phenotype in Vav2 ($Vav2^{-/-}$) or Vav2/Vav3-deficient ($Vav2^{-/-}Vav3^{-/-}$) mice. Vav2/Vav3-deficiency is associated with progressive iridocorneal angle changes and elevation of IOP in mice. Subsequent selective loss of RGCs and progressive ONH cupping are associated with this elevated IOP, as has previously been demonstrated in other rodent models of glaucoma [24]. The finding that Vav2-deficiency alone results in a glaucoma phenotype suggests that the absence of Vav2 plays a critical role in the development of this phenotype. Despite our finding that Vav3-deficiency did not result in either iridocorneal angle changes or elevated IOP, the more severe glaucomatous phenotype demonstrated in $Vav2^{-/-}Vav3^{-/-}$ mice as compared with $Vav2^{-/-}$ mice is consistent with an additive effect.

A number of induced glaucoma models have been established in rats and mice [24]. Each model has advantages and disadvantages, related to factors such as the ease of inducing elevated IOP, the magnitude, duration and variability of elevated IOP, and secondary effects on the eye. Due to the ease of genetic manipulation, mouse models are becoming increasingly popular over those in rats. Despite the lack of a lamina cribosa as found in human eyes, the mouse is a good genetic model to study the pathogenesis of human glaucoma as aqueous physiology and anterior segment anatomy are similar to that found in humans [25].

Other spontaneous models of glaucoma have been described in mice, most notably in DBA/2J mice. The pigmentary glaucoma phenotype demonstrated in the DBA/2J mice has been extensively studied at genetic, clinical, morphological and pathological levels [26–29]. A limitation of this model is that the elevated IOP phenotype is not primary but secondary due to the systemic pigment dispersion syndrome with the associated mutations in the *Gpnmb* and *Tyrp1* loci [26–30]. In these mice, recessive mutations in these 2 genes are associated with iris degeneration characterized by iris stromal atrophy and pigment dispersion with subsequent reduced outflow facility secondary to pigment and cell debris. Therefore, it is difficult to tie-in the identified mutations to the pathogenesis of any primary form of human glaucoma.

The Vav2/Vav3-deficient mouse has several characteristics which make it particularly useful as an animal glaucoma model. The elevated IOP occurs spontaneously in these genetically manipulated mice and does not require the ocular manipulation necessary in induced models. The frequency of the ocular phenotype is high and onset occurs at a relatively young age. In addition, ocular hypotensives commonly used to treat human glaucoma show efficacy in lowering IOP in this model. The most significant advantage of this mouse glaucoma model is that the deleted genes, Vav2 and Vav3, are well-focused targets that have been studied over 20 years providing a useful starting point for further investigation of the potential molecular mechanisms underlying this phenotype.

Several aspects of this model of spontaneous glaucoma will require further study and clarification, although we speculated from our histological results and the correlation between elevated IOP and angle status changes that anatomic angle closure is the possible mechanism for elevated IOP in this model. While progressive angle closure may be the etiology prior to elevated IOP in mice lacking Vav2 and Vav3 function, it may alternatively be a subsequent change related to other alterations in angle structures which might also affect aqueous humor outflow. In addition, since the expression of Vav2 and Vav3 was detected in ocular tissues other than those comprising the iridocorneal angle, it will be necessary in future studies to consider how their deficiency in these tissues might have potentially contributed to the spontaneous glaucoma phenotype in any way.

While so far there are several reports of glaucoma associated candidate genes based on the single nucleotide polymorphisms (SNPs) study in the Japanese population [31–36], our data first suggest that *VAV2* and *VAV3* are susceptibility loci in Japanese primary open–angle glaucoma (POAG) cases. In addition, so far we could not find the report of non-Japanese glaucoma association case study that demonstrated *VAV2* and/or *VAV3* as candidate gene loci for glaucoma [37–43]. They demonstrated glaucoma associated candidate genes study with SNPs analysis focusing on the other specific target genes, although we are interested in the *VAV2* and/or *VAV3* glaucoma association study using the different populations. This work would be important investigation to be done.

Although our current findings do not address the molecular mechanisms underlying glaucoma phenotypes, it is interesting to consider possible mechanisms based on what is currently known about Vav protein function. The TM has been regarded as a key determinant of IOP and has been implicated as the major site of

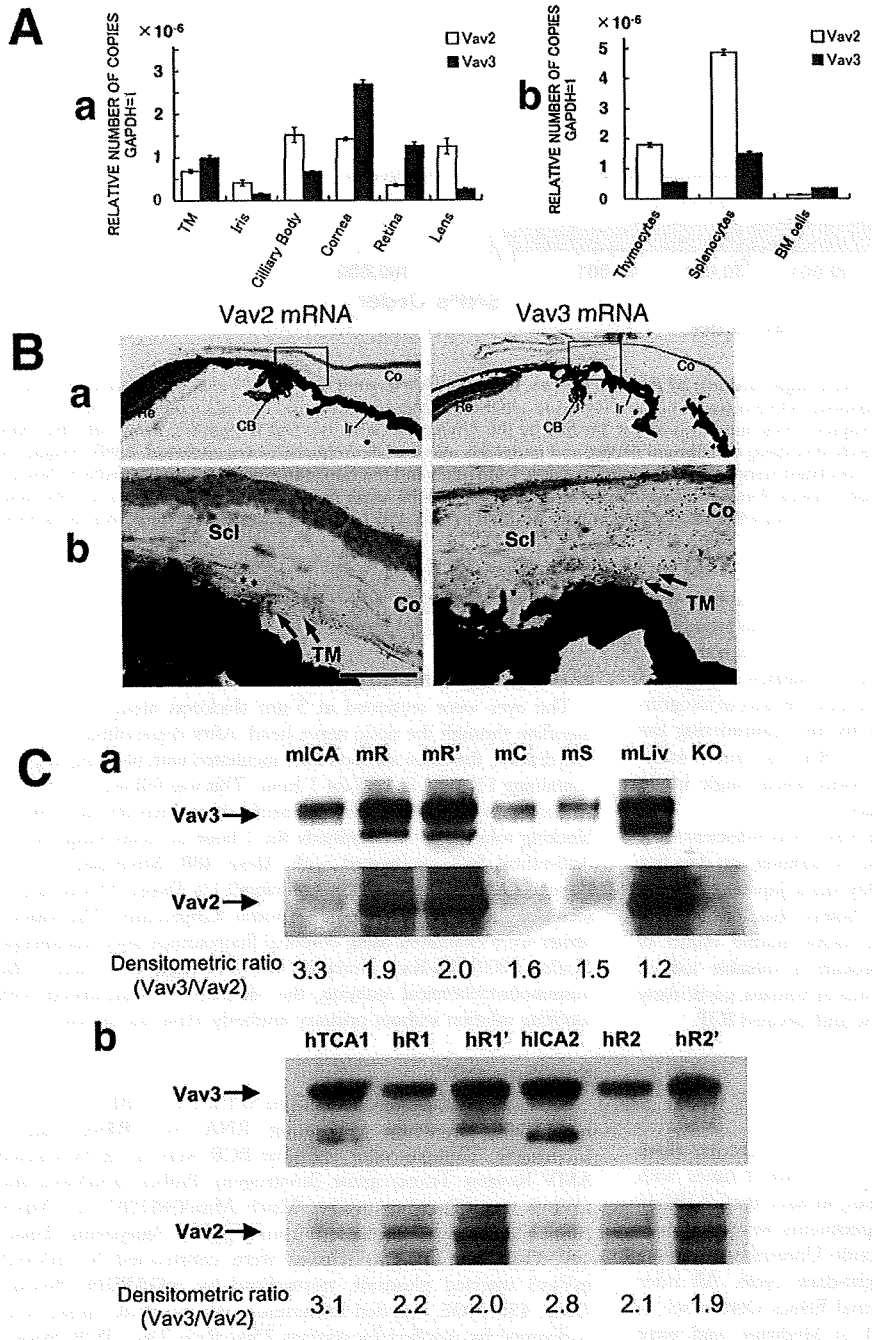

Figure 5. Vav2 and Vav3 expression in mouse and human eyes. A. Quantitative real time PCR analysis is performed for Vav2 and Vav3 mRNA expression study. The vertical axis is the copy number of Vav2 or Vav3 mRNA when that of mGAPDH is taken as 1. The assay method is absolute quantification (standard curve). **a.** Both Vav2 and Vav3 mRNA are expressed in all tissues of the murine eyes including the trabecular meshwork (TM), cornea, sclera, and retina. **b.** Vav2 and Vav3 mRNA expression level of murine immune cells. The levels of Vav2 and Vav3 expression in eye tissues are the same as those of the immune cells where Vav2 and Vav3 play the critical role. **B. a.** In situ hybridization analysis of emulsion-dipped sections display the distribution of Vav2 and Vav3 mRNA in the anterior chamber. The localization of Vav2 and Vav3 mRNA in trabecular meshwork(TM), ciliary body (CB), cornia(CO), iris(Ir), sclera (Scl) and retina(Re) by in situ hybridization. **b.** Vav2 and Vav3 mRNA expression are both detected in iridocorneal angle, such as TM (indicated by arrows in the photos). Scale bars, 50 μm. **C.** Expression of Vav2 and Vav3 proteins in mouse (**a**) and human (**b**) eyes. Vav2 and Vav3 proteins were detected in mouse or human ocular extracts (from two independent postmortem eye globe samples; at death age of 58 (1) and 87 (2)) by western blotting. Densitometric ratios (Vav3/Vav2) were shown under the blotting panels. mICA: mouse iridocorneal angle tissues, mR: mouse retina, mR': 3-fold increased loading mouse retina, mC: mouse cornea, mS: mouse sclera, mLiv: normal mouse liver(positive control), KO: Vav2/Vav3-deficient mouse as a negative control, hICA: human iridocorneal angle tissue,hR1: human retina 1, hR1': human retina1' (3-fold loading).
doi:10.1371/journal.pone.0009050.g005

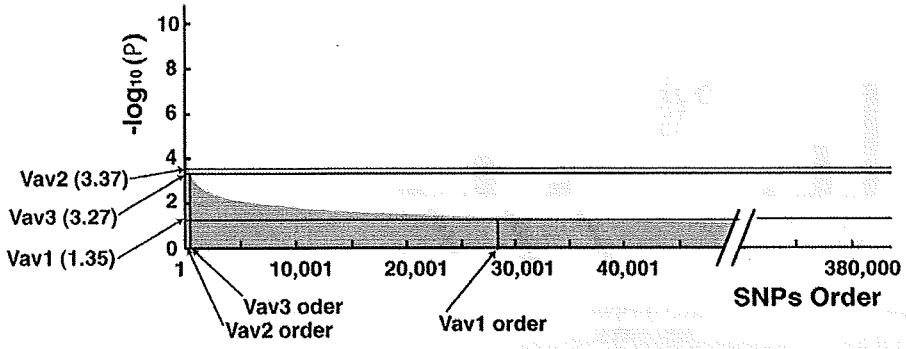

Figure 6. *VAV2* and *VAV3* genome-wide SNPs high ranking of *P*-value scores. Genome-wide ranking orders of *P*-value indicate that *VAV2* and *VAV3* are strongly susceptible genes with Japanese POAG cases. Clinically diagnosed Japanese POAG 100 cases and non-glaucoma age-matched 100 controls are examined for this study. The analysed SNPs number is about 380,000 by the Affymetrix GeneChip 500 K Mapping Array Set. The SNPs data under the 85% call rate, under 0.001 Hardy-Weinberg equilibrium (HWE), and under 5% minor allele frequencies are excluded. Allelic frequency $\chi 2$ test and genotypic frequency $\chi 2$ test are calculated respectively. The vertical axis is $-\log 10$ (*P*) and the horizontal axis is SNPs order which showed high scores from left to right. The Upper graph is alleric *P*-values distribution of *VAV2* analysis and the lower graph is genotypic *P*-values for *VAV3* and *VAV1* study. *VAV2* is located at high position in rank and *VAV3* also located at high position in rank. *VAV1* shows no association for POAG cases here.
doi:10.1371/journal.pone.0009050.g006

increased resistance to aqueous outflow which occurs in human glaucoma [44,45]. Recent findings indicate that signals emanating from integrins, key regulators of the actin cytoskeleton in trabecular meshwork cells, may be involved in control of outflow facility and Rho GTPases would be important downstream effectors of integrin-mediated actin cytoskeletal dynamics [4,46–48]. Considering the Vavs function as GEF, dysregulation of Rho is one possible mechanism by which pathology in the iridocorneal angle might result and is one that deserves further study.

In summary, we had demonstrated that Vav2/Vav3-deicient mice develop a spontaneous glaucoma phenotype. In addition, our data first suggest that *VAV2* and *VAV3* are susceptibility loci in Japanese primary open-angle glaucoma (POAG) cases. We believe that Vav2/Vav3-deficient mice will serve not only as a useful murine model of spontaneous glaucoma, but may also provide a valuable tool in understanding of the pathogenesis of glaucoma in humans, particularly the determinants of altered aqueous outflow and elevated IOP.

Materials and Methods

Mice

Vav3$^{-/-}$, *Vav2*$^{-/-}$ and *Vav2*$^{-/-}$*Vav3*$^{-/-}$ mice were described previously [15]. Mice were backcrossed at least 9 times with C57BL/6 mice (Clea Japan, Tokyo, Japan) to have the C57BL/6 background. All mice used in these experiments were bred and maintained in the SPF Facility of Hokkaido University Graduate School of Medicine in a 12-hour light-dark cycle. All mice experiments were approved by the Animal Ethics Committee of Hokkaido University Graduate School of Medicine and were conducted in accordance with the ARVO Statement for the Use of Animals in Ophthalmic and Vision Research.

Tissue Preparation and Histology

Eyes were quickly enucleated from each age group of knock-out mice and C57BL/6 wild-type control mice after deep anesthesia with pentobarbital sodium solution, then immediately fixed with solution of 2.5% glutaraldehyde (TAAB, EM Grade) in 10% formalin neutral buffer-methanol solution deodorized for anterior chamber study, or fixed with Davidson' solution for retinal analysis for 12 hours. Following this, the eyes were embedded in paraffin and dissected sagittally using a microtome into 5 μm sections. After deparaffinization and rehydration, the sections were stained with hematoxylin and eosin (Sigma).

Immunohistochemistry

The eyes were sectioned at 5 μm thickness along the vertical meridian through the optic nerve head. After deparaffinization and rehydration, the tissue sections were incubated with blocking solution containing 1% BSA in PBS for 1 hour. This was followed by 1 hour incubation with rabbit polyclonal antibody to myocilin at 1:200 in blocking solution as first antibody for 1 hour at room temperature. Anti-rabbit IgG conjugated with Alexa 488 (Molecular Probes, Eugene, OR) at 1:400 in PBS containing 0.1% Tween 20 was used as secondary antibody for 1 hour at room temperature. The stained tissues were examined using confocal fluorescence laser microscope (Radius 2000, Bio-Rad, Hercules, CA). For negative control of the immunohistochemical staining, the sections were incubated with blocking solution without primary antibody (data not shown).

Real Time PCR

Each tissue was freshly taken from SPF level C57BL/6 mice and immediately used for generating RNA by TRIzol reagent (Invitrogen). Templates for real time PCR were made by Cloned AMV Reverse Transcriptase (Invitrogen). Probes of mVav2 and mVav3 were TaqMan probes (Vav2: Mm00437287_m1, Vav3: Mm00445082_m1) purchased from Applied Biosystems (Foster city, CA). The standard curves were constructed by mVav2, mVav3 inserted plasmids, normalized by mGAPDH (Product Code: 4352339E, Applied Biosystems). All the PCR studies were performed by Applied Biosystems 7500 Real Time PCR System following the manufacturer's recommended procedures. The assay method was absolute quantification (standard curve).

In Situ Hybridization

The detailed procedure was described as previously [49]. Briefly, to detect mRNAs for Vav2 and Vav3, specific antisense oligonucleotide probes were synthesizedas follows:(2275–2319;45mers)5′-AGCTG-GAGACCGGCTTGAGGCC CTGCTGGTGGTTCGCTCCCG-AGA-3′ for Vav2 mRNA (GenBank accession No. NM_009500) and (2346–2302;45mers)5′–GTTGCCTGTTCTATTACCCCTCTG T CCAGCTGGCTGTTCTGGCTC-3′ for Vav3 mRNA (accession No. NM_020505). Oligonucleotide probes were labeled with [33P]

dATP using terminal deoxyribonucleotidyl transferase (Invitrogen, Carlsbad, CA). Under deep pentobarbital anesthesia, the eyeballs were freshly obtained from Adult C57BL/6J mice. Fresh frozen sections (20 μm thickness) were cut with a cryostat (CM1900, Leica, Nussloch,Germany) and mounted on glass slides precoated with 3-aminopropyltriethoxysilane. Sections were exposed to Nuclear Track emulsion (NTB-2, Kodak) for 5 weeks. Emulsion-dipped sections were stained with methyl green pyronine solution. The specificity of the hybridizing signals was verified by the disappearance of signals when hybridization was carried out with sense probes.

Western Blotting

Mouse Ocular Tissue Dissection: 8-week male C57BL/6J mice (Jackson Laboratory, ME) were used for ocular tissue samples. The animals were euthanized by carbon dioxide inhalation in an induction chamber. The globes were promptly enucleated after euthanization and washed in ice-cold PBS. Ocular tissues were microscopically dissected. Dissection of Postmortem Human Eye Globes: Human eyes without previous eye diseases including glaucoma were acquired from a local eye bank (Heartland Lions Eye Banks; Columbia, MO) within 6 hours post-mortem. Dissected mouse and postmortem human ocular tissues were lysed in a tissue extraction buffer (BioChain, CA). The concentration of protein supernatants was determined by a protein assay kit (Bio-Rad, CA). Rabbit polyclonal anti-mouse Vav2 (1:1000) (Santa Cruz Biotechnology, CA), monoclonal anti-human Vav2 (1:2000) (Cell Signaling Technology, MA), polyclonal anti-mouse and anti-human Vav3 (1:3000 for each) (Millipore, CA) antibodies were used for detection.

Intraocular Pressure (IOP) Measurement

IOP was measured using the TonoLab rebound tonometer for rodents (Tiolat i-care, Finland) according to the manufacturer's recommended procedures. All IOP measurements were performed between 10 AM and noon in conscious condition. Mice were gently restrained first by hand and placed on a soft towel bed on the desk and usually appeared calm and comfortable. These data were confirmed to be reproducible by three additional different independent studies (n = 20).

Evaluation of Eye Drop Medications for High Intra-Ocular Pressure of Vav2Vav3-Deficient Mice

Vav2$^{-/-}$*Vav3*$^{-/-}$ mice were housed in SPF barrier facility in standard lighting conditions (12-hour light-dark cycle). The 7–9 week after birth mice were used for the experiment. Four independent experiments were carried out to confirm the results reproducible.

Preparation and Application of Ophthalmic Solution

Latanoprost was purchased from Cayman Chemical Co. (Ann Arbor, MI) and dissolved in its vehicle solution (0.02% benzalkonium chloride, 0.5% monosodium phosphate monohydrate, 0.6% disodium hydrogen phosphate dihydrate and 0.4% sodium chloride). With a micropipette, 3 μl of PG analogue (latanoprost; prostaglandin F2α) solution or vehicle was randomly applied to the eyes of *Vav2*$^{-/-}$*Vav3*$^{-/-}$ mice. Before administration, IOP was measured with the tonometer from 10–12 AM and then the PG analogue 0.005% 3 μl or vehicle solution was applied in a masked manner. Evaluation of IOP-lowering effect was performed by measuring the IOP with the tonometer at 3 hours after drug instillation also in a masked manner. Furthermore, two different mechanistic medications, 3 μl of timolol maleate (0.5%, Merck, Whitehouse Station, NJ) or 3 μl of dorzolamide hydrochloride (1%, Trusopt; Merck), was also tested, respectively, after measuring the IOP under the same conditions as those of the Latanoprost application. Evaluation of IOP-lowering effects was performed by measuring the IOP with tonometer at 2 hours after drug instillation under blinded test protocols. Y-27632 was purchased from Carbiochem (La Jolla, CA) and dissolved in its vehicle solution (phosphate buffered saline). Y-27632 (1 mM) or vehicle solution was administered to the central cornea as a 3 μl drop by pipetting in a masked manner. Evaluation of IOP-lowering effect was performed by measuring the IOP with the tonometer at 1 hour after drug instillation.

Statistical Analysis of IOPs

Data are reported as means ± S.D. Two-tailed Student's t-test was used to compare between two groups of results. Differences between any two groups were regarded as significant when $P<0.01$(**) or $P<0.05$ (*).

Disease Associated Genome-Wide Analysis

One hundred clinically-diagnosed cases (male 46; female 54) with primary open-angle glaucoma over 30 years of age (mean age, 71.60 years; SD, 9.33 years) and non-glaucoma age-matched controls (mean age, 66.71 years; SD, 12.00 years) in a Japanese population were examined for this study. Informed consent was obtained from all participants, and the procedures used conformed to the tenets of the Declaration of Helsinki. Genomic DNAs were isolated from the peripheral blood of the POAG cases and age-matched controls for genotyping analysis. Genotyping was performed using the Affymetrix GeneChip Human Mapping 500 K Array Set (Affymetrix Services Laboratory, California). We omitted the SNP data under an 85% call rate, under 0.001 Hardy-Weinberg equilibrium (HWE), and under 5% minor allele frequency. Data analysis was performed using the LaboServer System (World Fusion, Tokyo Japan). An allelic frequency χ^2 test and genotypic frequency χ^2 test were calculated, respectively with respect to risk allele. The Odds ratio was calculated in three manners such as per allele odds ratio, heterozygote odds ratio, and homozygote odds ratio. Relative risk was also calculated, the same as for the odds ratio. The most significant SNPs were chosen in this report to evaluate the association of *VAV2*, *VAV3*, and *VAV1* in the cases.

Supporting Information

Figure S1 The comparison of intraocular pressures in age matched wild-type inbred C57BL/6 mice, wild-type littermate controls, and Vav2 and Vav3 heterozygous mice (Vav2$^{+/-}$, and Vav3$^{+/-}$). Intraocular pressures (IOPs) were measured using the TonoLab rebound tonometer for rodents from 6-week to 12-week, as described in the Methods. The phenotype of littermate wild-type mice was identical to that of the "inbred" C57BL/6 strain. The phenotype of Vav2 and Vav3 heterozygous mice were similar to that of wild-type. n = 20.
Found at: doi:10.1371/journal.pone.0009050.s001 (0.45 MB TIF)

Figure S2 The correlation between elevated IOP and angle changes in Vav2/Vav3-deficient mice. The IOP was measured in 7-week-old Vav2/Vav3-deficient (Vav2$^{-/-}$Vav3$^{-/-}$) mice (n = 20), followed by examination of the angle status by histology. While Vav2$^{-/-}$Vav3$^{-/-}$ mice with elevated IOP displayed histological evidence of angle closure, mice without elevated IOP showed either normal open angles or evidence of angle changes, angle closure or peripheral anterior synechiae. The mean and standard deviation of IOP in wild-type mice at 7-week-old (n = 18) were 13.7±3.12 mmHg, respectively. The 95th percentile of those